SYNTHESIS OF PRECURSORS FOR MOLECULAR ELECTRONICS

BY

ANGELA D. BROADNAX

A Dissertation Submitted to the Graduate Faculty of

WAKE FOREST UNIVERSITY GRADUATE SCHOOL OF ARTS AND SCIENCES

in Partial Fulfillment of the Requirements

for the Degree of

DOCTOR OF PHILOSOPHY

Chemistry

August, 2018

Winston-Salem, North Carolina

Approved By:

Mark E. Welker, Ph.D., Advisor

Oana D. Jurcheschu, Ph.D., Chair

Scott Geyer, Ph.D.

Willie L. Hinze, Ph.D.

Amanda C. Jones, Ph.D.

Acknowledgements

I'd like to thank Dr. Welker for being such a supportive and wise mentor. I am so grateful that you allowed me to join your research lab in 2013. I appreciate your patience and willingness to work with me for five years. You have taught me what it means to be a great leader in that you are quick to take-action- never procrastinating, you are a problem solver, and most importantly you are an expert in your field. Thanks to the Welker lab (Ron, Partha, Pamela, Emily, Lee, Jason, Nuwan, KyungMin, Taylor, Andrew, and Surya) for being like family to me. We have had some awesome times of which I will never forget. Ron, thanks for making my years in graduate school hilarious. KyungMin, thanks for being you-an amazing young lady and friend. Andrew, thanks for working so diligently to further along the molecular rectifier project. You are going to be an excellent graduate student. Dr. Amanda Jones, my other mentor, thanks for not only serving on my committee but for always encouraging and supporting me throughout my graduate career. Dr. Hinze, thanks for serving on my committee. I appreciate your unique insight as an analytical chemist. Dr. Geyer, thanks for serving on my committee and for always smiling and chatting with me during my breaks from thesis writing. Dr. Jurcheschu, thanks for serving as chair of my committee and for supporting me throughout this process. You inspire me because you are a woman, a great mentor, and you have such a positive personality. Zach, I am grateful to have worked with you. Thanks for never hesitating to share your knowledge. Dr. Franks, thanks for introducing me to the world of organic chemistry research. You are such a great mentor and motivator. I appreciate all that you've done for me over the years. Finally, I'd like to thank God for my wonderful parents, Earlean and Frankie Broadnax, for being so loving and supportive. Thanks for all that you've done from birth up until

now. Thank you for taking care of Zahra while I went into lab and stayed up late working on my dissertation. You are the best!!!

Dedicated to my daughter, Zahra A. Broadnax and my nephew, Vincent Galloway; my two loves ❤

Table of Contents

List of Figures

List of Schemes

List of Tables

List of Abbreviations

AC	Alternating current
AFM	Atomic force microscopy
BTBT	[1]Benzothieno[3,2-b]benzothiophene
CV	Cyclic voltammetry
DC	Direct current
DFT	Density Functional theory
EGaIn	Eutectic gallium-indium
HOMO	Highest occupied molecular orbital
HRMS	High resolution mass spectrometric
LB	Langmuir Blodgett
LC-MS	Liquid chromatography-tandem mass spectrometry
LUMO	Lowest unoccupied molecular orbital
MO	Molecular orbital
NMR	Nuclear magnetic resonance
OFET	Organic field-effect transistor
R	Rectification ratio
SAM	Self-assembled monolayer
STM	Scanning tunneling microscopy

μ	Field effect mobility

Abstract

The design of molecular rectifiers is one of the major topics of research in molecular electronics, however the relationship between the molecular structure and the electrical characteristics of molecular rectifiers is not fully understood. To elucidate this relationship, we synthesized and examined the electrical properties of fluorinated benzalkylsilane self-assembled monolayers (SAMs) of varying lengths and terminal groups. The rectification ratios were determined to be as high as ~200 and we also found that the rectification ratio correlates positively with the strength of the molecular dipole moment particularly for shorter chain molecules. Based on this data, we sought to design short chain benzalkylsilane SAMs with strong electron withdrawing and strong electron donating terminal groups. We hypothesized that terminations with these groups would give us enhanced rectification ratios based on their large dipole moments. Rectification ratios were found to be as high as 2635. These values to our knowledge are the highest reported for small molecule rectifiers assembled on silicon substrates.

Much of the work toward the study of molecular rectifiers has been done with ferrocene terminated alkanethiol SAMs. While these molecules present tremendous potential for molecular electronic devices, exhibiting rectification ratios as high as 200; synthesis is often complex, involving a five to six step synthesis. Additionally, the metal surface to which they assemble requires a time and cost intensive template stripping process. To circumvent these challenges, we have prepared four new ferrocenyl silanes in one or two simple chemical steps. These molecules were assembled as SAMs onto silicon wafers, which are nearly atomically flat as grown, with no additional fabrication steps. We

found that these SAMs can rectify current when incorporated in molecular diodes, with R values as high as 150 being obtained.

CHAPTER 1

INTRODUCTION TO MOLECULAR ELECTRONICS

1.1 Motivation

The field of molecular electronics involves the use of molecules as semiconductors in place of conventional solid state (inorganic) devices. Conventionally, as electronic devices have increased in performance and complexity, the number of components in an integrated circuit has scaled exponentially as per Moore's law.[1] Indeed, in 1965 Gordon E. Moore, the co-founder of Intel correctly predicted that the number of transistors on an integrated circuit device would double every 2-3 years because of shrinking device sizes. The miniaturization of these devices is now beginning to approach its limits as scaling down to sub nanometer sizes increases defects and cost of fabrication. Because single molecules constitute the smallest stable structures known, the idea of molecular electronics arose to address the challenges faced with the miniaturization of electronic circuits. Additionally, molecular electronics offers mechanical flexibility, low-cost fabrication, and tunable molecular functionality, properties that make it appealing for several applications including flexible displays, electronic paper, sensors, renewable energy sources, and numerous medical applications. Two examples of molecular electronics are molecular rectifiers (diodes) and organic thin film transistors which will be discussed in detail in chapters 4 and 5, respectively.[2]

1.2 Molecular Assemblies

Implementation of molecule designed electronic devices is based on the assembly of an individual or many molecules in an ordered fashion on a substrate (ie. Au, SiO_2). Due to the difficulty of arranging a single molecule on a surface, molecular assemblies have been employed. Two widely used examples of molecular assemblies in the field of molecular electronics are the Langmuir-Blodgett (LB) technique and Self-Assembled Monolayers (SAMs). These two techniques are attractive because they allow for a high density of molecules to be assembled onto a substrate simultaneously. Once the monolayers are placed in between electrodes, the structural and electrical properties of the junctions can be evaluated using standard methods of characterization such as contact angle measurements, cyclic voltammetry, and atomic force microscopy (AFM).

1.2.1. Langmuir-Blodgett monolayers

The LB technique, named after Irving Langmuir and his research assistant Katharine Blodgett, is one of the earliest models of 'supramolecular' assembly[3,4]. In this method, a single layer of molecules is formed on a liquid surface, usually water, before being transferred to a solid support to form a thin film with the thickness of a constituent molecule. When this process is repeated, multilayers of molecules form. The molecules used must be amphiphilic, having two parts: a hydrophilic, polar head group and a hydrophobic, non-polar hydrocarbon tail. When amphiphilic molecules are dissolved in a volatile organic solvent (chloroform, hexane, toluene, etc) and placed at the air-water interface, they arrange to cover the entire water surface area. Following evaporation of the solvent, a loosely packed monolayer is formed, whereby the hydrophilic ends interact

strongly with water (via dipole-dipole or hydrogen bonding interactions) and the hydrophobic tail protrudes from the water surface. The hydrophobic tail must be large enough so that it does not dissolve in the water layer. A true indicator of a Langmuir monolayer is an isotherm of surface pressure as a function of the area per molecule. Surface pressure can be defined as changes in the surface tension [4]of water upon covering it with molecules, and it can be recorded during compression of the film. [5] Figure 1.1, illustrates the 3 isotherm regions described by Oliviera[6]: (a) a zero pressure region usually referred to as "gaseous", (b) a region in which the molecules are in contact but not closely packed, and (c) a region of ordered and closely packed molecules .[7]

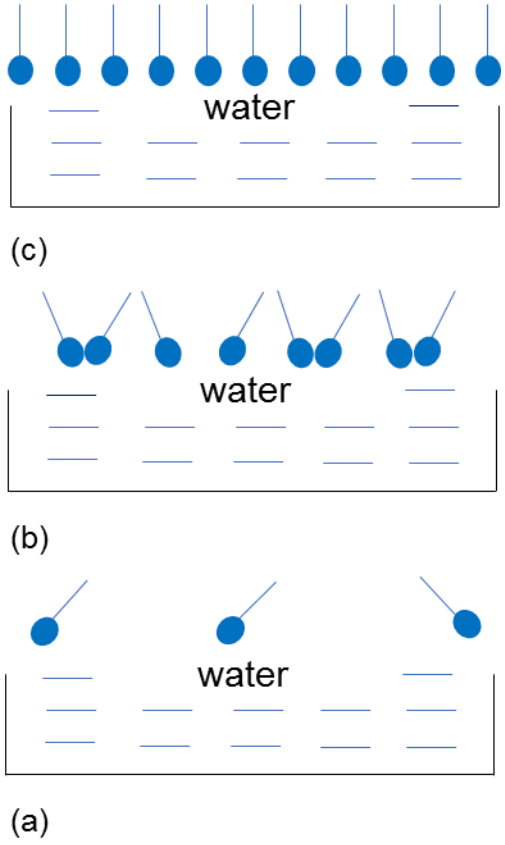

Figure 1.1. Three isotherm regions: (a) gaseous phase, (b) liquid-expanded phase, and (c) condensed phase.

Pulling a solid substrate through the interface results in the molecules being deposited on to the surface. The main advantage of the LB technique is the ability to control surface coverage of the molecules in the film as they are being deposited on the substrate. However, LB films are limited in that molecules are physisorbed and thus they do not have strong bonding to the electrode surface. The nature of the interaction between the molecule and the electrode surface can impact charge transport through a molecular junction. Lindsay et al. previously showed that for alkyl-thiol systems, current flow through the alkyl chain is greater when covalently bonded to the electrode surface versus when the chain is physisorbed.[8]

1.2.2. Self-assembled monolayers by chemisorption

Self-assembled monolayers (SAMs) are molecular assemblies formed by vapor or liquid phase adsorption of molecules with a strong affinity to the surface of a substrate.[9] The self-assembling molecules can be divided into three parts as illustrated in Figure 1.2: 1) Head group, i.e. $–SiOCH_3$. Forms the chemical bond with surface atoms of the substrate; 2) Alkyl chain, i.e. $–(CH_2)_n$. The alkyl chain is responsible for interchain van der Waals interactions; and 3) Terminal functional group, i.e. –R. The terminal group is replaced by different functional groups to provide electrical function in molecular electronic devices. [10] During the assembly process, strong chemical bonds are formed between the molecular "head groups" and the substrate surface resulting in stable and robust monolayers. Additionally, van der Waals interactions between neighboring alkyl chains help to ensure dense interchain packing thus, further stabilizing the monolayer.

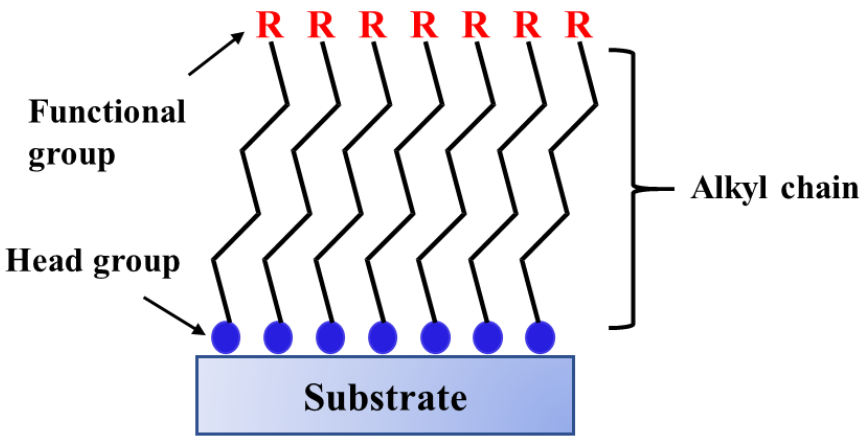

Figure 1.2. Self-assembled monolayer includes a head group chemisorbed to the substrate surface, an alkyl chain, and a terminal functional group.

The formation of a complete monolayer is dependent on the type of the molecule and its concentration, solvent, substrate metal, temperature, etc. In the beginning stages of monolayer formation, a low density of the molecules will adsorb in a disordered and randomly distributed state on the surface. Over time (e.g. minutes to days), the molecules will align in a uniform manner with the "head groups" on the substrate and the "tail groups" far from the substrate.[11]

There are two main types of self-assemblies which are classified by the type of molecule and substrate to which they bind. They include the following:

Alkanethiol monolayers on metal substrates:

Alkanethiols have become the most popular group of molecules for SAMs due to their greater solubility and high speed of assembly. They readily bind to noble metals such as gold, silver, copper, palladium, platinum, and mercury. However, gold is most often utilized since it does not oxidize at ambient conditions. A disadvantage of gold substrates

however, is the rough surface which can cause defects at gold grain boundaries, step edges and vacancy islands[12]. These imperfections would interfere with the alignment of molecules thus hampering the monolayer order. To circumvent this challenge, Whitesides et al. have developed ultra-smooth films of gold, silver, platinum, and palladium via a template stripping method[12].

Alkoxy or chlorosilane monolayers on Si/SiO_2 substrates:

Despite receiving less attention than alkanethiols, organosilane SAMs have many advantages, namely their dense packing ability, smooth substrate surface which eliminates the need for cost and time intensive template stripping, and the availability of knowledge and input from the very successful silicon industry that can be used to develop integrated molecular devices or hybrid devices[13].

Organosilane monolayers are made up molecules such as $RSiX_3$, R_2SiX_2, or R_3SiX (where R = Carbon chain and X = Cl, OCH_3 or OCH_2CH_3) chemisorbed onto hydroxylated silicon dioxide surfaces. During adsorption, the SiX head group reacts in an aqueous environment with the -OH groups via hydrolysis, resulting in Si-O-Si bonds at the surface. Due to the tight packing of the monolayers, Si-O-Si bonds are also formed between neighboring molecules via condensation reactions (See Figure 1.3). The degree of monolayer coverage is dependent on the type of molecules, particularly the length of the alkyl chain, and experimental conditions such as the temperature, pressure[14], and solvent[13].

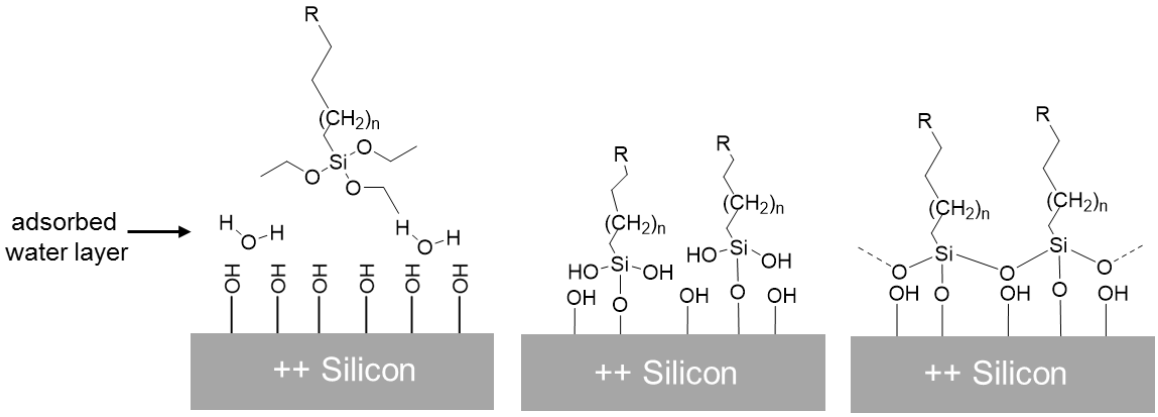

Figure 1.3. Organosilane chemisorption process adapted from [10]

1.3 Characterization of self-assembled monolayers

1.3.1. Contact Angle

Contact angle measurements can be used to determine the quality of SAMs by examining the hydrophilicity and hydrophobicity of a surface[15]. Upon placing a drop of water on the surface, the angle between the film and liquid droplet is measured. The measured angle indirectly reflects the degree of surface order and can indicate the incorporation of functional groups, for the contact angle changes with varying film composition[16]. For example, a contact angle measurement of a closely packed SAM will have a slightly different contact angle from that of a disordered SAM. For SAMs terminated with hydrophilic groups such as -OH or -COOH, the water droplet will make a smaller contact angle as the water will interact more with the hydrophilic surface. Conversely, SAMs terminated with hydrophobic terminal groups will have a larger contact angle due to the absence of attraction to water.

1.3.2. Cyclic Voltammetry

Cyclic voltammetry (CV) is a powerful electrochemical tool used to study electron-transfer in redox active species on the surface of an electrode. The molecules on the electrode surface have a direct impact on the electrochemical process. Thus, if a film monolayer is sufficiently thick, charge transport can be hindered due to separation between the electrode surface and the redox active molecules. Alternatively, if the film is small and the redox active species are near the electrode, electrons can tunnel through it. Hu et al. demonstrated this concept using several thiol-end tetraphenylporphyrins both with and without metal centers. Porphyrins with metal centers (redox active) resulted in greater electron flow than those without metals. Additionally, when the thiol-end link spacer (alkyl group) increased from 3 CH_2's to 10, the electron transport ability of the SAMs decreased because of the increased insulator properties of the alkyl chain[17]. This phenomenon may be explained by two different charge transport mechanisms: 1) electrons are transported from the gold electrode directly through the space between the two porphyrin molecules or from the defect of the molecule; and 2) electrons are transported from the SAM surface where electrons tunnel through the alkyl bridge and then through the alkyl ring. The latter is the likely mechanism for the porphyrins because the sulfurs do not allow the π orbitals to interact strongly with the conduction orbitals of gold electrodes. This orbital mismatch creates an energy barrier at the Au/SAM interface. The tunneling process has been used extensively to explain carrier injection through a bond particularly for metal-molecule-metal junctions with energy mis-alignment[18,19].

1.4 Fabrication of molecular junctions with liquid metals drop junctions

To measure the electrical properties of SAMs, it is necessary to attach metal electrodes on each side of the molecules. Electrical contact between the molecules and the bottom electrode is made upon assembly. Thus, finding a suitable method to contact the top of the SAM is imperative for completing the junction and establishing electrical conductivity. Chiechi et al. have defined four important characteristics for an ideal top electrode. They are as follows: The electrode should 1) make conformal but non-damaging physical contacts, 2) readily form micrometer sized diameter contacts, to minimize the contribution of defects in the SAM to current, 3) form without specialized equipment and 4) be non-toxic[20]. Several top contact methods have been used such as evaporated metal contacts, scanning probe (Scanning tunneling microscopy (STM)) and conductive probe (atomic force microscopy (AFM)), conductive polymer contacts, and liquid metal contacts. Each type of junction has both pros and cons. In this work, we will focus on the liquid metal junctions as they form reproducible, non-damaging contacts to the SAM surface[21].

1.4.1. The Hg Top Electrode

Mercury has been used as reliable top contact in molecular junctions consisting of metal-SAM-SAM-metal junctions since 1997. The two monolayers making up the SAM-SAM interface are necessary for preventing direct contact between the two metal electrodes, which would lead to amalgam formation. The conductivity of these junctions is controlled by interactions (i.e. hydrogen bonding, covalent bonding, and van der Waals interactions) present between the electrodes and SAMs.

Despite its ability to make conformal, non-damaging contact to the SAM surface, mercury drop based junctions are highly toxic and have a large (~250μm^2) contact area, which increases the likelihood of defects in the SAMs.

1.4.2. The EGaIn Top Electrode

Recently, Whitesides et al. successfully used a new liquid metal top electrode formed from conically shaped tips of EGaIn (a liquid eutectic alloy, 75.5 wt% Ga and 24.5 wt% In). The EGaIn electrode is non-toxic, it can be formed into non-spherical shapes with small (1-100μm) diameter contact areas, and it does not require a second SAM layer as it is coated by a layer of Ga_2O_3.

1.5 Electron Transport

As mentioned previously, a monolayer of molecules sandwiched between metal electrodes allows one to study its electrical characteristics. However, understanding the mechanism of charge transport is non-trivial. Several factors influence how charges (electrons or holes) travel across the molecule/electrode interface of the junction such as temperature, molecular size and structure, the energy and position of the molecular orbitals, the type of bonding in the metal-molecule junctions, and the energy alignment of the molecular orbital levels with the Fermi energy level of the electrodes.

Tunneling

The most common mechanism of electron transport for molecular rectifiers is tunneling. Tunneling is a quantum mechanical phenomenon where an electron passes through a barrier with a given height and thickness. Its probability depends on the barrier

width and availability of the unoccupied states (lowest unoccupied molecular orbital (LUMO) or conduction band) on the other side of the barrier. In the context of a molecular junction, if the molecular orbitals cannot be accessed (highest occupied molecular orbital (HOMO)-LUMO gap is too large), the electron is forced to tunnel through the space between the two electrodes (barrier width). The tunneling current shows an exponential dependence on the barrier width (length of the molecule) as represented by the Simmons equation:

$$J = J_0 e^{-\beta d} \tag{1.1}$$

Where: J = current density (A/cm^2), J_0 = constant, dependent on the applied voltage, thickness, and height of the energy barrier, β = constant, proportional to a square root of the barrier height and mass of electron (nm^{-1}), d = barrier width. Tunneling is a temperature independent process thus, experimentalists can measure the current of a molecular junction at various temperatures to determine its mode of electron transport.

1.6 Molecular Rectifiers

1.6.1. Introduction to Molecular Rectifiers

A rectifier or diode is an electrical circuit component that allows more current to flow in one direction than the other. As such, an ideal rectifier would allow current to flow unimpeded in only one direction[22,23]. Rectifiers are important because they are one of the main building blocks of alternating current (AC) to direct current (DC) converters[22]. Because virtually all digital electronics require DC and most homes and buildings are powered by AC, rectifiers are used extensively for this purpose.

The molecular rectifier, proposed by Aviram and Ratner[24] in 1974 was the origin of molecular electronics. The Aviram-Ratner diode example shown in Figure 1.4, involves a donor-σ-acceptor molecule connected symmetrically to two metal electrodes[25]. The sigma bridge located between the donor and acceptor, effectively adds a large tunnel barrier to the backbone so that the energy levels of the donor and acceptor will not interact with each other and thus can be treated separately[24,26]. According to Aviram and Ratner, this donor-σ-acceptor system will conduct current asymmetrically-as a rectifier when a voltage is applied in the positive direction but not in the opposite direction. For this to occur, the lowest unoccupied molecular orbital (LUMO) of the acceptor unit and highest occupied molecular orbital (HOMO) of the donor unit must be close to the Fermi level of the electrodes (demonstrated in Figure 1.5a)[23,24,26]. In order for electrons to flow, a voltage of proper polarity must be applied, so that the Fermi level of the left electrode is higher than the LUMO level of the acceptor and the HOMO level of the donor is higher than the Fermi level of the right electrode as shown by the energy level diagram in Figure 1.5b.[27] Under reverse bias, electrons do not flow unless a much higher voltage is applied. Thus, rectification occurs at a specific range of applied voltage.

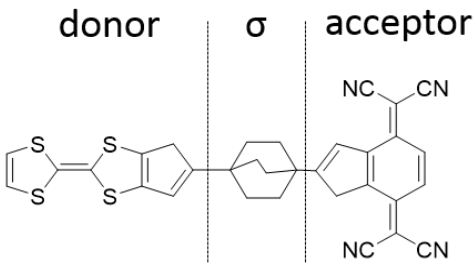

Figure 1.4. Example of an Aviram-Ratner diode

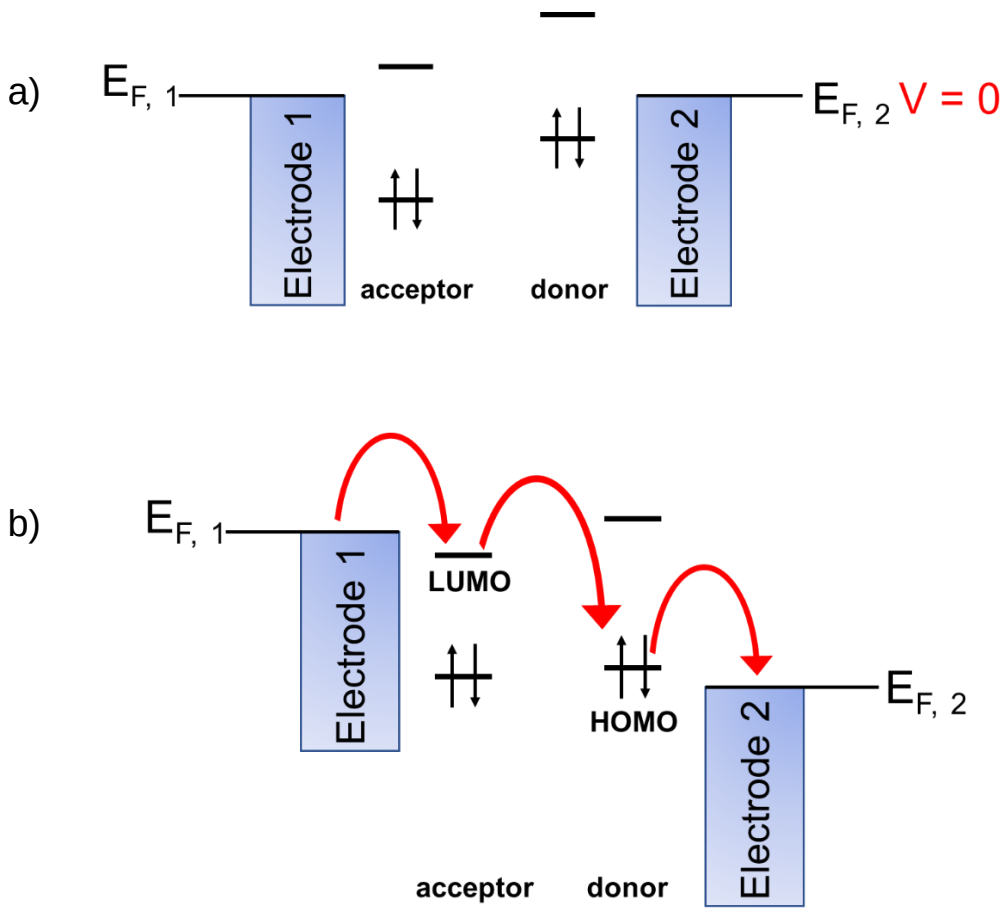

Figure 1.5. Energy levels of electrodes, acceptor, and donor when a) no voltage is applied and b) voltage of one polarity is applied.

As a result of these electrical requirements, few experiments have been successful at producing single molecule diodes with optimal rectification ratios (R) as R ≈ 5 orders of magnitude for solid state devices and R ≈ 1 order of magnitude or less for molecular rectifiers[5,28]. The rectification ratio (Equation. 1) is defined as the ratio between electrical currents through the junction in the conducting and insulating directions where J = current density (A/cm^2) and V = voltage (V).

$$R = \left|\frac{J(V_{conducting})}{J(V_{insulating})}\right| \tag{1.2}$$

Due to the energy level alignment requirements of the donor-σ-acceptor model, a commercial molecular diode has not been reported[29]. Furthermore, it wasn't until 1997 that Metzger et al. confirmed the first molecular diode with electron transport from donor to acceptor. The molecular rectifier consisted of Langmuir-Blodgett (LB) films of zwitterionic γ-(n-hexadecyl)quinolinium tricyanoquinodimethanide, $C_{16}H_{33}$Q-3CNQ (Figure 1.6). The $C_{16}H_{33}$Q-3CNQ system is actually a T-D^+-π-A^- molecule, where T is the hydrophobic $C_{16}H_{33}$ tail used to promote good LB films, D^+ is the quinolinium moiety, π is the π-electron bridge, and A^- is the tricyanoquinodimethamide (3CNQ) moiety[23,30]. The monolayer was supported by Al top and bottom electrodes each connected to an Au wire by eutectic Ga/In. The 3CNQ(A^-) end was placed next to the bottom electrode which was grounded and the bias voltage was applied to the top electrode. A larger current flowed at the positive bias voltage above 1.0 V, indicating that electrons preferentially flowed in one direction from the acceptor, 3CNQ(A^-) to the donor, quinolinium(D^+). Almost half (17 out of the 39) of the devices short circuited, either because of monolayer defects or because the eutectic Ga/In made defects. Out of the working devices, four yielded rectification ratios between 2.4 and 26.4[30]. As the cycle of J-V measurements was repeated, the *R* value decreased steadily indicating film instability.

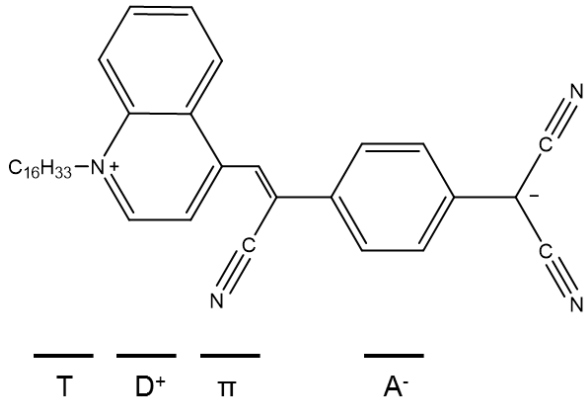

Figure 1.6. γ-(n-hexadecyl)quinolinium tricyanoquinodimethanide ($C_{16}H_{33}$Q-3CNQ), a T-D^+-π-A^- molecule, where T is the hydrophobic $C_{16}H_{33}$ tail used to promote good LB films, D^+ is the quinolinium moiety, π is the π-electron bridge, and A^- is the tricyanoquinodimethamide (3CNQ) moiety[23,30]

The pioneering work of Metzger et al has prompted researchers to address new issues concerning molecular diodes such as device performance and reproducibility. SAMs by way of chemisorption to the bottom electrode and physisorption to the top electrode has shown promise in improving film stability while increasing *R* values by up to 2-3 orders of magnitude[28,31–33]. Additionally, experimentalists have found enhanced rectification from systems containing a single π bonded component bonded to an insulating bridge rather than two π bonded components (donor-acceptor) which presumably makes the requirements for rectification more tangible.

History of the Single Conducting Molecular Orbital Rectifier

A mechanism based on the one conductive molecular orbital (MO) was proposed by Williams et al. and Baranger et al[26,34]. For rectification to occur in molecular tunneling junctions with a single conducting molecular orbital, either the HOMO or LUMO must be close in energy to the Fermi levels of the electrodes and asymmetrically coupled to one of the electrodes (i.e., in closer spatial proximity to one electrode than the other). Figure 1.7 outlines the mechanism for the molecular rectifier (SC_{10}-phenyl-C_2S (Figure 7 a)) proposed by Williams et al. They achieve rectification with the LUMO, located to one side of the molecule at forward bias (Figure 1.7c), where the applied potential allows conduction through the MO before tunneling through the insulating alkyl chain. At reverse bias (Figure 1.7d), most of the applied potential is dropped over the alkyl chain resulting in an overall reduced conductivity. Although, other mechanisms of rectification have been

proposed for such diodes[35,36], Nijhuis et al.'s extensive work with molecular rectifiers corroborates with the groups of Williams and Baranger et al.

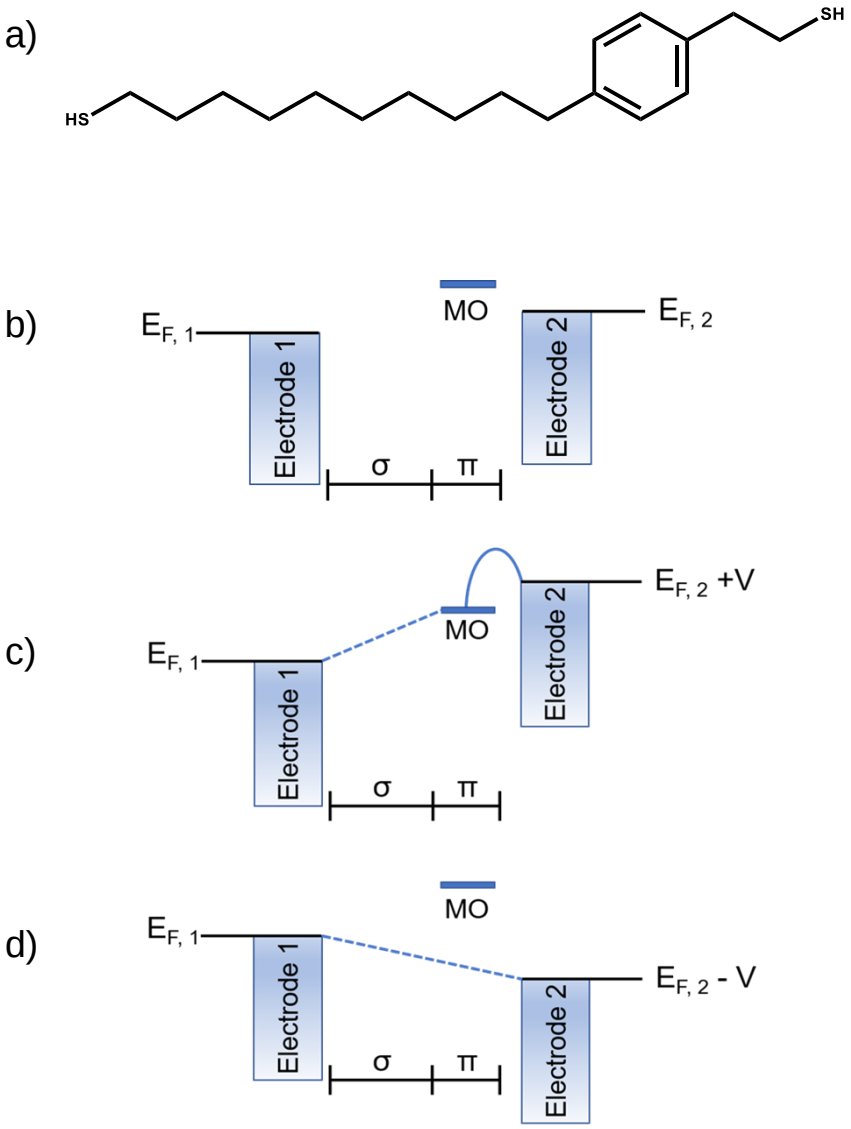

Figure 1.7. a) SC_{10}-phenyl-C_2S molecular rectifier, proposed by Williams et al., with an asymmetrically coupled LUMO. Energy level diagrams of electrodes and a single π bonded component at b) zero bias c) forward bias- conduction occurs through the MO then tunnels through the alkyl chain, d) reverse bias- the potential drops along the entire length of the molecule and thus only tunneling occurs. Adapted from Zach Lamport's dissertation.

Experimental work with molecular diodes possessing one conducting molecular orbital

Nijhuis et al. have reported on the rectification of ferrocenyl-alkanethiol SAMs assembled on a template-stripped silver (Ag^{TS}) bottom electrode and contacted to eutectic gallium/indium (EGaIn 75.5%, Ga 24.5% by weight) top electrode (Figure 1.8)[23,32]. A eutectic Ga/In is a liquid at room temperature but its spontaneously formed surface oxide (Ga_2O_3) surface gives it non-Newtonian properties that allow it to be molded into conical shaped tips. These tips formed soft electrical contacts with 11-(ferrocenyl)-1-undecanethiol and formed stable tunneling junctions in high (70-90%) yields[37]. The bottom electrode was grounded and ±1V was applied to the top electrode. The rectification was determined to be ~100 for the ferrocenyl-alkanethiol SAMs. In contrast, alkanethiol junctions with the same thickness but lacking the ferrocene head group, that is, $SC_{10}CH_3$ and $SC_{14}CH_3$, showed much smaller rectification ratios[32]. Theoretical calculations determined that the HOMO of the ferrocene head group was responsible for the rectification of current. The HOMO level followed the potential of the Fermi level of the Ga_2O_3/EGaIn electrode; it overlapped energetically with both Fermi levels of the electrodes only in the negative bias voltage.

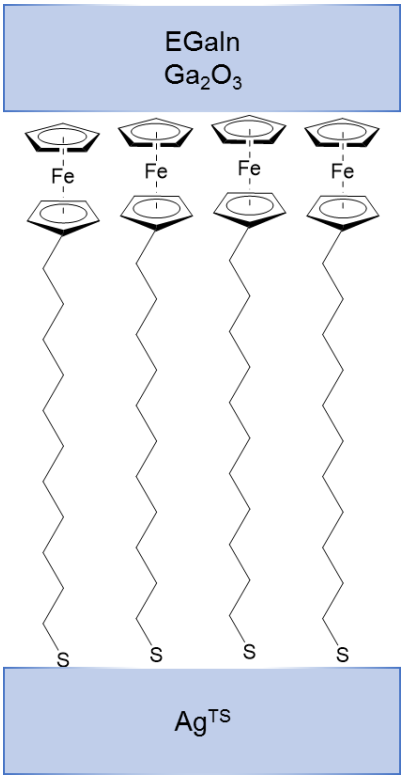

Figure 1.8. A schematic of ferrocenyl alkanethiol SAMs sandwiched between Ag and Ga_2O_3/EGaIn metal contacts.

The relationship between the monolayer composition and electronic function of ferrocene-alkanethiol SAMs of $S(CH_2)_nFc$ (n = 6-15 and Fc = ferrocenyl) was studied[23,38]. The bottom electrode was grounded, and bias voltage was applied to the EGaIn top electrode. A larger current was observed at the negative voltage. Self-assembled monolayers with n = 9, 11, and 13 have the largest *R* values, believed to be due to the odd-even effect. Tilt angle measurements of the Fc units with respect to the surface normal was on average ~5º smaller (that is, the Fc units were less tilted) for SAMs with n_{odd} on the substrates than for SAMs with n_{even}. Additionally, the more upright SAMs with n_{odd} on the substrate resulted in tighter packing due to more favorable interchain interactions. These SAMs gave high yields of working devices with small leakage current at the reverse bias. The low levels of leakage current at the reverse bias resulted in SAMs with large *R* values.

The rectification ratio can be increased by using more than one conducting molecular orbital. Yuan et al., prepared biferrocenyl-alkanethiol SAMs of $SC_{11}Fc_2$ on a Ag substrate with an EGaIn top electrode[39]. The substrate was grounded, and bias voltage was applied to the top electrode. A large current flowed at the negative voltage. The rectification ratio was determined to be 1000, a value that is 10 times larger than the single ferrocenyl-alkanethiol SAM. Charge transport was believed to be due to sequential tunneling involving two orbitals, the HOMO and HOMO-1 which are coupled to the top electrode. The biferrocenyl-alkanethiol SAM with two conduction orbitals also had much higher currents in the on state than SAMs with only one conduction orbital[39].

Bipyridyl Rectifier

Similar to the early work of Nijhuis et al., 2,2'-bipyridyl-terminated n-alkanethiol SAMs of $S(CH_2)_{11}$-4-methyl-2,2'-bipyridyl were made on a Ag substrate and contacted by

an EGaIn top electrode[23,40]. The bottom electrode was grounded, and the bias voltage was applied to the top electrode. A larger current flowed at the positive voltage, which was opposite to that of the ferrocene SAM. Theoretical calculations revealed that charge transport was dominated by the LUMO of the bipyridyl unit which was coupled to the EGaIn top electrode. The difference in the conducting molecular orbitals for each system explains the opposite direction of rectification. Rectification ratios as high as 85 were obtained.

1.7 Organic Thin Film Transistors

1.7.1. Introduction

Organic thin film transistors (OTFTs), best described as voltage controlled current switches, are the basic building blocks of organic electronic applications[41–43]. Unlike silicon-based transistors, which require high temperature processes (>800 ºC), organic transistors can be manufactured at or near room temperature, and thus on flexible polymeric substrates and even on paper[41]. Because OTFTs have the advantage of being inexpensive, flexible, and light weight, they have been used in applications such as identification tags, sensors, switches, etc.[41]

The fundamental structure of an OTFT (Figure 1.9) consists of an organic semiconductor layer bridging source and drain electrodes[44,45]. The third electrode, the gate is separated by a dielectric layer (insulating) from the OTFT. When a voltage (current) is applied to the gate, a flow (channel) of electrical current streams between the source and drain at the semiconductor layer and the transistor is "on". The channel is "turned off" when no voltage is applied to the gate. The current (I_D) in the channel can be controlled by

independently tuning the voltage applied between the gate and source (V_{GS}) and between the drain-source (V_{DS}).

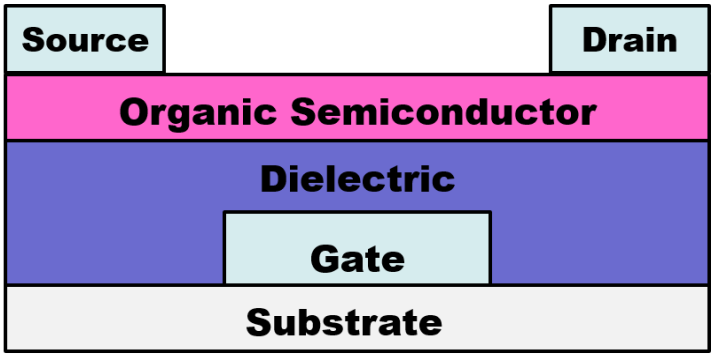

Figure 1.9. Schematic representation of an organic thin-film transistor.

1.7.2. Charge carrier transport

The semiconducting property that allows for organic molecules to conduct electric charge is molecular conjugation (i.e. the presence of alternating single and double bonds between covalently bound carbon atoms). Conjugation causes the delocalization of one of the four valence electrons of each carbon atom that participates in the conjugated system, resulting in the efficient transport of electronic charge along a conjugated molecule[41].

Organic transistors usually consist of conjugated molecules arranged in an ordered fashion on a thin film[41]. Because the intermolecular bonds in organic solids consist of relatively weak van der Waals interactions, charge transport does not typically extend over the entire volume of the solid but are localized to a finite number of molecules or sometimes to individual molecules. The carrier mobility of electrons traveling through the organic semiconductor is thus determined by the ease with which electrons are transported from one molecule to the next under an applied electric field. The carrier mobilities of OTFTs

vary greatly depending on the structure of the semiconductor, its impurities, and the molecular arrangement of the solid. Through molecular engineering and by inducing semi-crystalline order through better control of the film formation, the mobilities of OTFTs can be enhanced[41].

1.7.3. Organic Semiconductors

Highly extended polyacenes such as pentacene have driven the field of organic electronics for several years.[46] Despite their high carrier mobilities, without bulky substitutions, polyacenes easily undergo air oxidation limiting their use in practical electronic applications. One approach to enhance the stability of polyacenes is to insert heteroaromatics such as thiophenes into the acene structure, giving thioacenes.[47] The incorporation of thioacenes into OTFTs has resulted in films with good stability and high carrier mobilities, a result of their lower HOMO energy level. Among the thienocene based organic semiconductors, [1]Benzothieno[3,2-b]benzothiophene (BTBT) derivatives have shown the best performance in terms of high mobility, air stability, and good reproducibility.

1.7.4 [1]Benzothieno[3,2-b][1]benzothiophene-based Organic Thin Film Transistors

Organic thin film transistors incorporating C8-BTBT have shown to be superior over others.[48] The C8-BTBT molecule possesses an eight-carbon alkyl chain at the 2 and 7 positions on the BTBT core structure. The linear alkyl chain positively influences charge

mobility by enhancing solution processability and by facilitating interchain interactions which lead to greater π-π interactions in the BTBT core layers.

Minemawari et al., developed a double shot ink jet method that combines an antisolvent and a solution of C8-BTBT, respectively to produce organic semiconducting films of high crystallinity[49]. Mixing of the antisolvent and solution of C8-BTBT within a confined area on the substrate led to the self-organization of single crystals which is important for achieving high carrier mobility. Using this method, OTFTs with single crystals of C8-BTBT resulted in mobilities as high as 31.3 cm^2/Vs, the 3rd highest mobility reported to date.

More recently, Bao et al., reported on the ultra-high mobility of a C8-BTBT based OTFT grown by a novel off centre spin-coating method[50]. A solution of C8-BTBT and a polystyrene binder was dispensed onto a glass substrate located near the edge of a turntable and spun at a much higher speed than normal. Despite its large-scale impracticality, this method produced a record high mobility of 43 cm^2/Vs, the highest value obtained for small-molecular organic semiconductors.

1.7.5. Operating Voltages

Organic thin film transistor mobility has improved significantly and several polymeric and small molecule semiconductors can be compared with their silicon counterparts[51–53]. However, contemporary OTFTs suffer from low charge carrier mobility and high operating voltages. Most OTFTs operate at voltages above 40V, with mobilities lower than $1cm^2/Vs$ (for comparison, the carrier mobilities in silicon are above 10^2

cm^2/Vs)[41]. The operating voltage, V_{GS} is dictated by the required charge density Q in the OTFT channel, at the interface between the dielectric and the semiconductor, which, in turn, is induced by the gate-source voltage. The operating voltage and the charge density are related by the areal capacitance of the dielectric layer, C_i:

$$Q = C_i V_{GS} = \frac{\varepsilon_0 \varepsilon_r}{d} V_{GS} \quad (1.3)$$

Where ε_0 and ε_r are the permittivity of the free space and the relative permittivity of the dielectric respectively, and d is the thickness of the dielectric. Thus, a large operating voltage is not a desirable property of OTFTs and can be reduced by decreasing the dielectric thickness or employing dielectric materials with high ε_r (high permittivity). Creating high quality dielectrics thinner than 100 nm is challenging due to the inherent formation of pinholes that lead to high leakage currents[54–56]. A large number of high-k dielectrics; inorganic[54–56] and organic[55,57–59], were developed and used in organic devices; while an acceptable solution for polymeric devices, this approach fails with small molecule organic semiconductors because Fröhlich polarons form and localize charges, limiting transport[60].

1.8 Dissertation Outline

Chapter 2 summarizes the design and synthesis and electrochemical characterization of 9 novel fluorinated benzalkylsilane self-assembled monolayers (SAMs). The monolayer was sandwiched between bottom and top contacts of highly doped silicon and eutectic gallium/indium (EGaIn), respectively. Their electrical properties were measured, and the rectification strength was found to be comparable to other optimal performing molecular

diodes. Additionally, we found that the rectification ratio correlates positively with the molecular dipole moments.

Chapter 3 summarizes the design, synthesis, and electrochemical characterization of benzalkysilanes having electron withdrawing and electron donating terminations. This chapter also includes the synthesis of benzalkylcarboxylic and benzalkylphosphonates for comparison to benzalkylsilanes. Based on our work with fluorinated benzalkylsilanes, we hypothesized that these molecules would give us enhanced rectification ratios but in opposite directions based on the directions of their dipole moments. Rectification ratios up to 2635 were obtained, which is the highest reported for small molecular diodes formed on silicon.

Chapter 4 summarizes the synthesis and electrochemical characterization of ferrocenealkylsilanes. The ferrocenyl silanes used in this work can be easily prepared in one to two simple steps from readily available ferrocene carboxaldehyde. We found that the molecular diodes obtained from these molecules can exhibit current rectification ratios as high as 150. The ease of processing coupled with the excellent rectification behavior makes these compounds very attractive for molecular electronics applications.

Chapter 5 summarizes the synthesis and chemical characterization of polyacenes and polyheteroacenes such anthracene and [1]benzothieno[3,2-b][1]benzothiophene (BTBT) derivatives, respectively for use as semiconductors in organic thin film transistors.

CHAPTER 2

FLUORINATED BENZALKYLSILANE MOLECULAR RECTIFIERS

Zachary Lamport‡, **Angela Broadnax**†, Mark Welker†, and Oana Jurcheschu‡

†Department of Chemistry, Wake Forest University, Winston-Salem, NC 27109,

‡Department of Physics, Wake Forest University, Winston-Salem, NC 27109

This work was adapted from Zachary A. Lamport**, Angela D. Broadnax**, David Harrison, Katrina J. Barth, Lee Mendenhall, Clayton T. Hamilton, Martin Guthold, Timo Thonhauser, Mark E. Welker, and Oana D. Jurchescu. *Scientific Reports* **6**, 38092 (2016)

2.1 Introduction

Molecular electronics has been an area of great interest as device technology closes on the limits of the often-mentioned Moore's law, with consumer-available technology already in the tens of nanometers range. The idea of molecular electronics was proposed as a means to surpass the challenges present in downscaling existing technologies[61–63]; however, commercially viable examples have yet to be introduced.[29,64–67] Since 1974, when Aviram and Ratner proposed the first rectification mechanism for a molecular structure containing a donor-acceptor pair separated by a σ-bonded tunnelling bridge, the field has witnessed spectacular growth.[24] A rectifier is a device which allows a large amount of current to pass through at one bias while restricting current flow at the opposite bias. While the above mentioned theoretical work extrapolated the inorganic solid-state p-n junction miniaturized to the size of a single molecule and relied on the manipulation of the molecule's energy levels, several different mechanisms for enhanced rectifications have subsequently been proposed.[36,68–70] Further experimental work has also demonstrated that the donor-acceptor pair may not always be necessary, and that systems with a single π-bonded component and a σ-bonded insulating chain can provide a more consistent, as well as a greater degree of, rectification.[10,38,71] Significant research effort was dedicated toward the examination of both single-molecule and molecular assemblies as rectifiers, with clear advantages exhibited by both.[72–75] Single molecule devices allow for a direct comparison with the theoretical calculations due to the lack of complexity in such systems. Nevertheless, Nijhuis *et al.* produced convincing arguments for the observed rectification in ferrocene-terminated alkanethiolate molecules assembled on surfaces in monolayer patterns.[25,32,76] Other self-assembled monolayers and Langmuir-Blodgett films provide

ease of fabrication due to the molecule's penchant for assembling on a well-chosen surface. This allows for the formation of many devices on a single substrate simultaneously and without the difficult alignment task present in single-molecule structures. The research to improve the rectifying behaviour of molecular diodes, however, has proceeded mostly by trial and error and a relation between the molecular structure and resulting strength of rectification has not been clearly demonstrated.

In this work, we developed nine new fluorinated benzalkylsilane molecules of varying internal molecular dipole due to the imposed length and termination, and we studied their electrical properties in relation to their chemical structure. We incorporated the self-assembled monolayers (SAMs) composed of these molecules into molecular diodes and obtained high yields and reproducible rectification ratios as high as 200, with good bias stress stability. We calculated the molecular dipole using density functional theory (DFT) and we found that the rectifying behavior is stronger in the case of short molecules and is enhanced by the internal dipole. Our results provide evidence that the molecular structure impacts the electrical properties of molecular diodes through the internal dipole characteristic to each molecule and may promote a rational design of compounds that can function as high-performance molecular rectifiers.

2.2 Experimental

2.2.1 Instrumental Analysis and Chemicals

The proton nuclear magnetic resonance (^{1}H NMR) spectra were obtained using a Bruker Avance 300 MHz spectrometer operating at 300.1 MHz or a

Bruker Avance 500 MHz spectrometer operating at 500.1 MHz. ^{13}C NMR spectra were obtained using a Bruker Avance 300 MHz spectrometer operating at 75.5 MHz. ^{1}H and ^{13}C NMR spectra were referenced to the residual proton or carbon signals of the respective deuterated solvents. All elemental analyses were performed by Atlantic Microlabs Inc., Norcross, GA. High-resolution mass spectrometry was performed at the Mass Spectrometry Facility at Northwestern University, Evanston, IL. All reactions were carried out under an atmosphere of nitrogen. Aminoundecyltriethoxysilane was purchased from Gelest and used as received. Deuterated solvents were purchased from Cambridge Isotope Laboratories and dried over molecular sieves. Aminopropyltriethoxysilane and the benzaldehydes were purchased from Aldrich Chemical Company and used as received. Anhydrous sodium sulfate and HPLC grade hexane were purchased from Fisher/Acros and used as received.

2.2.2 Synthesis and Characterization

(*E*)-1-(4-trifluoromethyl)phenyl)-*N*-(11-(triethoxysilyl)undecyl)methanimine (1). Anhydrous Na_2SO_4 (4.0 g) was added to a solution of 4-trifluoromethylbenzaldehyde (0.350 g, 2.01 mmol) in HPLC grade hexane (7 mL). A solution of aminoundecyltriethoxysilane (AUDTES) (0.738 g, 2.211 mmol) in HPLC grade hexane (7 mL) was added dropwise with stirring to the resulting mixture over 12 min. After 3 h, some additional precipitate was noted, the solution was decanted, the residue was rinsed with additional hexane (5 mL) and hexane was removed in vacuo. Compound **1** was isolated as a clear liquid (0.719 g, 1.47 mmol, 73%): ^{1}H

NMR (300 MHz, $CDCl_3$) δ 8.31 (s, 1H), 7.83 (d, J = 6 Hz, 2H), 7.66 (d, J = 6 Hz, 2H), 3.81 (q, J = 6 Hz, 6H), 3.63 (t, J = 6 Hz, 2H), 1.70 (m, 2H), 1.61-1.26 (m, 18H) 1.22 (t, J = 6 Hz, 9H), 0.62 (t, J = 9 Hz, 2H); ^{13}C NMR (75.47 MHz, $CDCl_3$) δ 159.21, 139.46, 132.01 (q, J = 32.3 Hz), 128.20, 125.53 (q, J = 3.8 Hz), 123.96 (q, J = 270 Hz), 61.90, 58.29, 33.21, 30.79, 29.63, 29.58, 29.54, 29.44, 29.26, 27.36, 22.76, 18.31, 10.39. Elem. Anal. Calcd. for $C_{25}H_{42}F_3NO_3Si$: C, 61.32; H, 8.65; Found: C, 61.56; H, 8.84.

(*E*)-1-(3,5-bistrifluoromethyl)phenyl)-*N*-(11-(triethoxysilyl)undecyl)methanimine (2). Anhydrous Na_2SO_4 (4.0 g) was added to a solution of 3,5 bis(trifluoromethyl)benzaldehyde (0.121 g, 0.500 mmol) in HPLC grade hexane (7 mL) A solution of AUDTES (0.172 g, 0.515 mmol) in HPLC grade hexane (7 mL) was added dropwise with stirring to the resulting mixture over 12 min. After 3 h, some additional precipitate was noted and the solution was decanted, the residue was rinsed with additional hexane (5 mL) and hexane was removed in vacuo. Compound **2** was isolated as a light-yellow liquid (0.208 g. 0.373 mmol, 75%). ^1H NMR (300 MHz, $CDCl_3$) δ 8.35 (s, 1H), 8.18 (s, 2H), 7.90 (s, 1H), 3.81 (q, *J* = 7.0 Hz, 6H), 3.66 (t, *J* = 6.9 Hz, 2H), 1.70 (q, *J* = 6.9 Hz, 2H), 1.47 – 1.11 (m, 25H), 0.72 – 0.51 (m, 2H). ^{13}C NMR (75 MHz, $CDCl_3$) δ 155.29, 136.16, 130.61, 130.16, 129.94 (q, *J* = 33.6 Hz), 125.71, 122.85, 121.56, 121.04 (q, *J* = 272.7 Hz), 59.66, 56.16, 31.07, 28.55, 27.51, 27.43, 27.40, 27.29, 27.12, 25.23, 20.63, 16.17, 8.28. Elem. Anal. Calcd. For $C_{26}H_{41}NO_3F_6Si$: C, 56.00; H, 7.41; Found: C, 55.95; H, 7.35.

(*E*)- 1-(4-fluoro)phenyl)-*N*-(11-(triethoxysilyl)undecyl)methanimine (3). Anhydrous Na_2SO_4 (1.33 g) was added to a solution of 4-fluorobenzaldehyde (0.083 g, 0.670 mmol) in hexane (2.3 mL). A solution of AUDTES (0.245 g, 0.737 mmol) in hexane (2.3 mL) was added dropwise with stirring to the resulting mixture over 5 min. After 3 h, some additional precipitate was noted, the solution was decanted, the residue was rinsed with additional hexane (5 mL) and hexane was removed in vacuo. Compound 3 was isolated as a light-yellow liquid (0.136 g, 0.310 mmol, 46%). ^{1}H NMR (500 MHz, $CDCl_3$) δ 8.23 (s, 1H), 7.71 (dd, *J* = 8.4, 5.8 Hz, 2H), 7.08 (t, *J* = 8.6 Hz, 2H), 3.81 (q, *J* =7.0 Hz, 6H), 3.58 (t, *J* = 7.0 Hz, 2H), 1.77 – 1.58 (m, 2H), 1.48 – 1.14 (m, 25H), 0.69 –0.55 (m, 2H). ^{13}C NMR (126 MHz, $CDCl_3$) δ 164.14 (d, *J* = 250.3 Hz), 132.68 (d, *J* = 3.0 Hz), 129.83 (d, *J* = 8.6 Hz), 115.61 (d, *J* = 21.8 Hz), 77.27, 77.01, 76.76, 61.71, 58.29, 33.20, 30.92, 29.63, 29.59, 29.54, 29.45, 29.26, 27.36, 22.76, 18.31, 10.40. Elem. Anal. Calcd. for $C_{24}H_{42}FNO_3Si$: C, 65.56; H, 9.63. Found: C, 65.84; H, 9.60.

(*E*)-1-(3-fluoro-4-trifluoromethyl)phenyl)-*N*-(11-(triethoxysilyl)undecyl)methanimine (4). Anhydrous Na_2SO_4 (4.0 g) was added to a solution of 3-fluoro-4- trifluoromethyl)benzaldehyde (0.096 g, 0.500 mmol) in HPLC grade hexane (7 mL). A solution of AUDTES (0.172 g, 0.515 mmol) in HPLC grade hexane (7 mL) was added dropwise with stirring to the resulting mixture over 12 min. After 3 h, some additional precipitate was noted, and the solution was decanted, the residue was rinsed with additional hexane (5 mL) and hexane was removed in vacuo. Compound **4** was isolated as a clear liquid (0.237 g. 0.467 mmol, 93%). ^{1}H NMR (300 MHz, $CDCl_3$) δ 8.26 (s, 1H), 7.62 (m, 2H),

3.81 (q, *J* = 7.0 Hz, 6H), 3.64 (t, *J* = 6.9 Hz, 2H), 1.68 (q, *J* = 6.9 Hz, 2H), 1.47 – 1.11 (m, 25H), 0.62 (m, 2H). ^{13}C NMR (75 MHz, $CDCl_3$) δ 158.0 (dq, *J* = 256, 2.1 Hz), 157.9 (d, *J* = 2.0 Hz), 142.2 (d, *J* = 7.6 Hz), 127.4 (qd, *J* = 4.6, 1.4 Hz), 123.6 (d, *J* = 3.6 Hz), 122.4 (qd, *J* = 273, 1.2 Hz), 119.7 (dq *J* = 32.9, 12.6 Hz) 115.5 (d, *J* = 21.5 Hz), 61.74, 58.27, 33.18, 30.68, 29.61, 29.55, 29.51, 29.40, 29.24, 27.33, 22.75, 18.28, 10.39. Elem. Anal. Calcd. for $C_{25}H_{41}NO_3F_4Si$: C, 59.15; H, 8.14; Found: C, 59.15; H, 8.08.

(E)-1-(4-trifluoromethylphenyl)-N-(3-(triethoxysilyl)propyl)methanimine (5). Anhydrous Na_2SO_4 (3.0 g) was added to a solution of 4-trifluoromethylbenzaldehyde (0.235 g, 1.348 mmol) in HPLC grade hexane (5 mL). A solution of aminopropyltriethoxysilane (APTES) (0.328 g, 1.483 mmol) in HPLC grade hexane (5 mL) was added dropwise with stirring to the resulting mixture over 10 min. After 1.5 h, some additional precipitate was noted, the solution was decanted, the residue was rinsed with additional hexane (5 mL) and hexane was removed in vacuo. Compound **5** was isolated as a clear liquid (0.422 g, 1.12 mmol, 83%): ^{1}H NMR (300 MHz, $CDCl_3$) δ 8.30 (s, 1H), 7.82 (d, J = 6 Hz, 2H), 7.64 (d, J = 6 Hz, 2H), 3.83 (q, J = 6 Hz, 6H), 3.64 (t, J = 6 Hz, 2H), 1.85 (m, 2H), 1.24 (t,J = 6 Hz, 9H), 0.68 (t, J = 9 Hz, 2H); ^{13}C NMR (75.47 MHz, $CDCl_3$) δ 159.37, 139.48, 131.97 (q, J = 19.5 Hz), 128.17, 125.45, 123.94 (q, J = 162 Hz), 64.22, 58.31, 24.18, 18.21, 8.03. HRMS (APCI-ion trap) m/z: $[M + H]^+$ Calcd for $C_{17}H_{27}O_3NF_3SiH$ 378.1707; Found 378.1704.

(E)-1-(3,5-bistrifluoromethyl)phenyl)-*N*-(3-(triethoxysilyl)propyl)methanimine (6). Anhydrous Na_2SO_4 (3.0 g) was added to a solution of 3,5-bistrifluoromethylbenzaldehyde (0.242 g, 1.00 mmol) in hexane (5 mL). A solution of APTES (0.244 g, 1.10 mmol) in hexane (5 mL) was added dropwise with stirring to the resulting mixture for 5 min. After 1.5 h, with presence of hydrolyzed product precipitated, the solution was decanted, and hexane was removed in vacuo. Compound **6** was isolated as a clear liquid (0.376 g, 0.845 mmol, 85%). ^{1}H NMR (300 MHz, Chloroform-*d*) δ 8.35 (s, 1H), 8.18 (s, 2H), 7.91 (s, 1H), 3.84 (q, *J* = 7.0 Hz, 6H), 3.68 (td, *J* = 6.9, 1.1 Hz, 2H), 1.93 – 1.78 (m, 2H), 1.23 (t, *J* = 7.0 Hz, 9H), 0.73 – 0.65 (m, 2H). ^{13}C NMR (75 MHz, $CDCl_3$) δ 157.71, 138.26, 132.07 (q, *J* = 33.6 Hz), 123.18 (q, *J* = 272.6 Hz), 127.88, 123.72 (hept, *J* = 3.8 Hz), 64.17, 58.44, 24.12, 18.31, 8.12. HRMS (APCI-ion trap) m/z: $[M + H]^+$ Calc for $C_{18}H_{25}O_3NF_6SiH$ 446.1586; Found 446.1583.

(E)- 1-(4-fluorophenyl)-N-(3-(triethoxysilyl)propyl)methanimine (7). Anhydrous Na_2SO_4 (3.0 g) was added to a solution of 4-monofluorobenzaldehyde (0.150 g, 1.209 mmol) in HPLC grade hexane (5 mL). A solution of APTES (0.294 g, 1.330 mmol) in HPLC grade hexane (5 mL) was added dropwise with stirring to the resulting mixture over 10 min. After 1.5 h, some additional precipitate noted, the solution was decanted, the residue was rinsed with additional hexane (5 mL) and hexane was removed in vacuo. Compound **7** was isolated as a light-yellow liquid (0.345 g, 1.05mmol, 87%): ^{1}H NMR (300 MHz, $CDCl_3$) δ 8.23 (s, 1H), 7.70 (t, J = 6 Hz, 2H),

7.08 (t, J = 6 Hz, 2H), 3.82 (q, J = 6 Hz, 6H), 3.59 (t, J = 6 Hz, 2H), 1.82 (m, 2H), 1.22 (t, J = 6 Hz, 9H), 0.67 (t, J = 9 Hz, 2H); ^{13}C NMR (75.47 MHz, $CDCl_3$) δ 164.02 (d, J = 248.3 Hz), 159.49, 132.73, 129.93,115.62 (d, J = 21.8 Hz), 64.18, 58.39, 24.29, 18.32, 8.10. HRMS (APCI-ion trap) m/z: $[M + H]^+$ Calc for $C_{16}H_{27}FNO_3Si$ (M +) calcd: 328.1744; obs: 328.1748.

(E)-1-(3-fluoro-4-trifluoromethyl)phenyl)-N-(3-(triethoxysilyl)propyl)methanimine (8). Anhydrous Na_2SO_4 (3.0 g) was added to a solution of 3-fluoro-4- trifluoromethyl)benzaldehyde (0.384 g, 1.00 mmol) in HPLC grade hexane (5 mL). A solution of APTES (0.244 g, 1.10 mmol) in HPLC grade hexane (5 mL) was added dropwise with stirring to the resulting mixture over 10 minutes. After 1.5 h, the solution was decanted, and hexane was removed in vacuo. Compound (**8**) was isolated as a clear liquid (0.342 g. 0.865 mmol, 87%). ^{1}H NMR (300 MHz, Chloroform-*d*) δ 8.27 (s, 1H), 7.67 – 7.53 (m, 3H), 3.83 (q, *J* = 7.0 Hz, 6H), 3.65 (t, *J* = 6.5 Hz, 2H), 1.89 – 1.79 (m, 2H), 1.23 (t, *J* = 7.0 Hz, 9H), 0.70 – 0.64 (m, 2H). ^{13}C NMR (126 MHz, $CDCl_3$) δ 159.9(dq, *J* = 256, 2.1 Hz), 158.2 (d, *J* = 2.0 Hz), 142.2 (d, *J* = 7.7 Hz), 127.3 (qd, *J* = 4.6, 1 Hz), 123.7 (d, *J* = 3.6 Hz), 122.5 (qd, *J* = 270, 1.2 Hz), 119.7 (dq *J* = 32.9, 12.6 Hz) 115.4 (d, *J* = 21.5 Hz), 64.09, 58.37, 24.09, 18.25, 8.05. HRMS (APCI-ion trap) m/z: $[M + H]^+$ Calc for $C_{17}H_{25}O_3NF_4SiH$ 396.1618; Found 396.1612.

(E)-1-(pentafluorophenyl)-N-(3-(triethoxysilyl)propyl)methanimine (9). Anhydrous Na_2SO_4 (3.0 g) was added to a solution of pentafluorobenzaldehyde (0.133 g, 0.678 mmol) in hexane (8 mL). A solution of APTES (0.150 g, 0.678 mmol) in hexane (8 mL) was added dropwise with stirring to the resulting mixture over 10 min. After 1 h, additional precipitate was noted, and the solution was decanted, the residue was rinsed with additional hexane (5 mL) and hexane was removed in vacuo. Compound **9** was isolated as a light-yellow liquid (0.183 g, 0.458 mmol, 68%). ^{1}H NMR (500 MHz, $CDCl_3$) δ 8.38 (s, 1H), 3.83 (q, *J* = 7.0 Hz, 6H), 3.70 (t, *J* = 6.7 Hz, 2H), 1.93 – 1.75 (m, 2H), 1.23 (t, *J* = 7.0 Hz, 9H), 0.71 – 0.59 (m, 2H). ^{13}C NMR (126 MHz, $CDCl_3$) δ 149.16 (p, *J* = 2.5 Hz), 145.70 (ddtd, *J* = 256.0, 11.5, 7.6, 3.9 Hz), 141.85 (dtt, *J* = 256.9, 13.7, 5.1 Hz), 137.6 (dtdd, *J* = 253.1, 14.1, 6.0, 2.0 Hz), 111.30 (td, *J* = 12.0, 4.2 Hz), 65.77, 58.39, 24.03, 18.27, 7.90. HRMS (APCI-ion trap) m/z: $[M + H]^+$ Calc for $C_{16}H_{22}O_3NF_5SiH$ 400.1362; Found 400.1353.

2.2.3 Molecular Design of Rectifiers

The examined molecules were fluorine-substituted benzaldehyde imine-terminated trialkoxysilanes, designed such that each contains a triethoxysilane group that ensures the attachment on the Si/SiO_2 surface, an alkyl chain with either 3 or 11 CH_2 groups, a phenyl group to facilitate the formation of an "intermolecular top-link" to enhance ordering, and a fluorine-containing head-group providing different amounts and orientations of fluorine atoms.

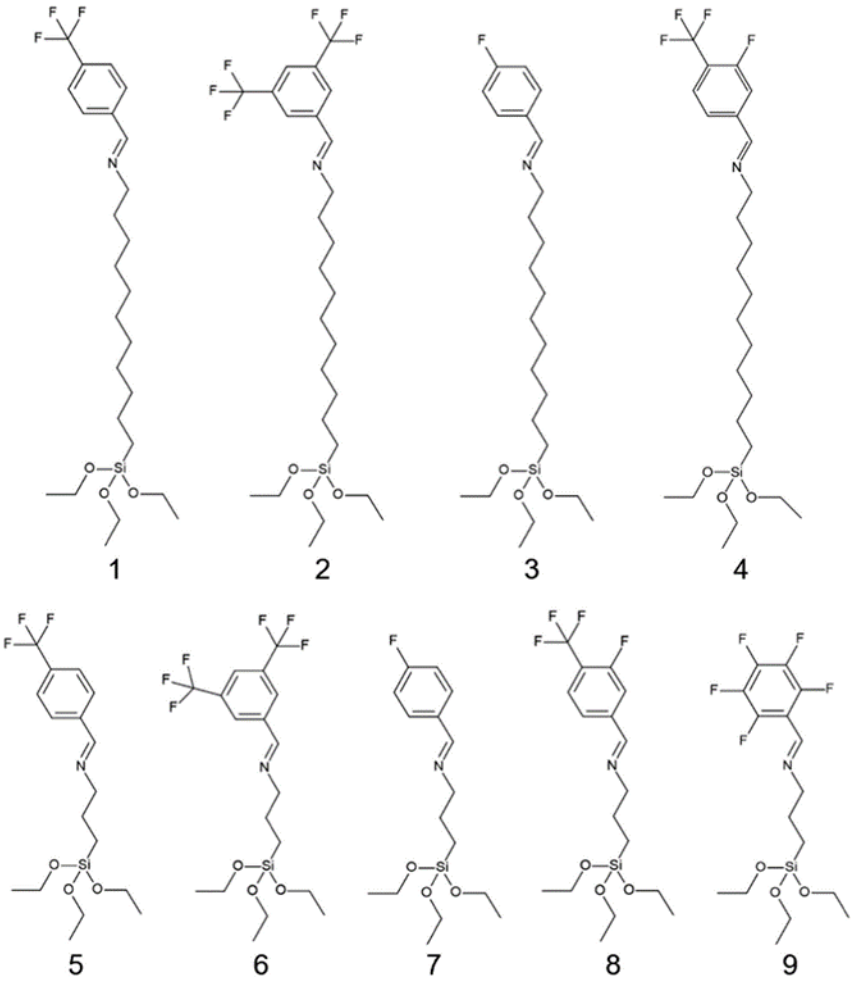

Figure 2.1. Chemical structures of molecules 1-9.

The chemical structures are included in Figure 2.1[77,78], as follows: (*E*)-1-(4-(trifluoromethyl)phenyl)-*N*-(11-(triethoxysilyl)undecyl)methanimine (molecule 1),(*E*)-1-(3,5-bis(trifluoromethyl)phenyl)-*N*-(11-(triethoxysilyl)undecyl)methanimine (molecule 2), (*E*)-1-(4- fluorophenyl)-*N*-(11-(triethoxysilyl)undecyl) methanimine (molecule 3), (*E*)- 1-(3-fluoro-4-trifluoromethyl) phenyl)-*N*-(11-(triethoxysilyl)undecyl)methanimine (molecule 4), (*E*)-1-(4-(trifluoromethyl)phenyl)-*N*-(3-(tri- ethoxysilyl)propyl)methanimine

(molecule 5), (*E*)-1-(3,5-bis(trifluoromethyl)phenyl)-*N*-(3-(triethoxysilyl) propyl) methanimine (molecule 6), (*E)*-1-(4-fluorophenyl)-*N*-(3-(triethoxysilyl)propyl) methanimine (mol- ecule 7), (*E*)- 1-(3-fluoro-4-trifluoromethyl)phenyl)-*N*-(3-(triethoxysilyl)propyl)methanimine (molecule 8) and (*E*)-1-(perfluorophenyl)-*N*-(3-(triethoxysilyl)propyl) methanimine (molecule 9). (*E*)-1-(perfluorophenyl)- *N*-(11-(triethoxysilyl)undecyl) methanimine (the long chain analogue of molecule 9) was also investigated; its properties, however, varied significantly from sample to sample, as well as for the same film, and therefore we decided not to include it in our analysis.

2.2.4 Synthesis Results and Discussion

The molecules were synthesized from amino trialkoxysilanes by using the condensation of commercially available amino alkyl triethoxysilanes with substituted benzaldehydes to prepare the precursors, following established procedures as illustrated in Scheme 2.1. The yields for all reactions were in the 68–87% range and the only purification of the products required after the reaction was filtration and removal of residual solvent under high vacuum. We will refer to molecules 1, 2, 3, and 4 as the "long molecules" (their lengths are between 2 and 2.2 nm) and molecules 5 through 9 as the "short molecules" (their lengths are between 0.9 and 1.1 nm). The length was evaluated using Spartan software, measured from the Si atom to the most distal atom of the head-group for the lowest energy conformer of each molecule.

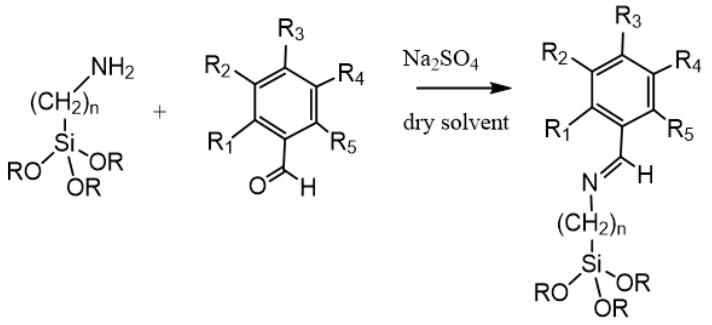

1 R = Et, n = 11, $R_3 = CF_3$, $R_{1, 2, 4, 5} = H$, 73%

2 R = Et, n = 11, $R_2 = R_4 = CF_3$, $R_{1, 3, 5} = H$, 75%

3 R = Et, n = 11, $R_3 = F$, $R_{1, 2, 4, 5} = H$, 46%

4 R = Et, n = 11, $R_3 = CF_3$, $R_2 = F$, $R_{1, 4, 5} = H$, 93%

5 R = Et, n = 3, $R_3 = CF_3$, $R_{1,2,4,5} = H$, 82%

6 R = Et, n = 3, $R_2 = R_4 = CF_3$, $R_{1,3,5} = H$, 85%

7 R = Et, n = 3, $R_3 = F$, $R_{1,2,4,5} = H$, 87%

8 R = Et, n = 3, $R_3 = CF_3$, $R_2 = F$, $R_{1, 4, 5} = H$,87%

9 R = Et, n = 3, R_1-$R_5 = F$, 68%

Scheme 2.1. Synthesis of molecules 1-9.

It is important to note that the reaction times for the "long" molecules (1-4) were twice as long than for the "short" molecules. This is not surprising because longer alkyl chains are bulkier and thus can hinder reactivity of the amino trialkoxysilanes with benzaldehydes. Additionally, longer alkyl chains facilitate greater van der Waals interactions between neighboring chains, stabilizing them.

Initially after examining the ^{13}C NMR spectra of these molecules we were puzzled because there were more peaks than expected in the aromatic region despite being able to assign all peaks in the ^{1}H NMR. However, we later found that the extra peaks were due to C-F coupling arising from the NMR active F19 isotope of the fluorine atoms on these molecules. Because the ^{13}CNMR pulse sequence lacked C-F

decoupling, C-F splitting was observed as illustrated in the aromatic region of the ^{13}C spectrum for molecule 4 (Figure 2.2). For example, carbon 7 is split by three fluorine neighbors so it is a quartet. Similarly, carbon 6 is a doublet because it is split by 1 fluorine neighbor. Also note the multiplicities of the other carbons due to the 1, 2 and 3 bond J coupling to ^{19}F.

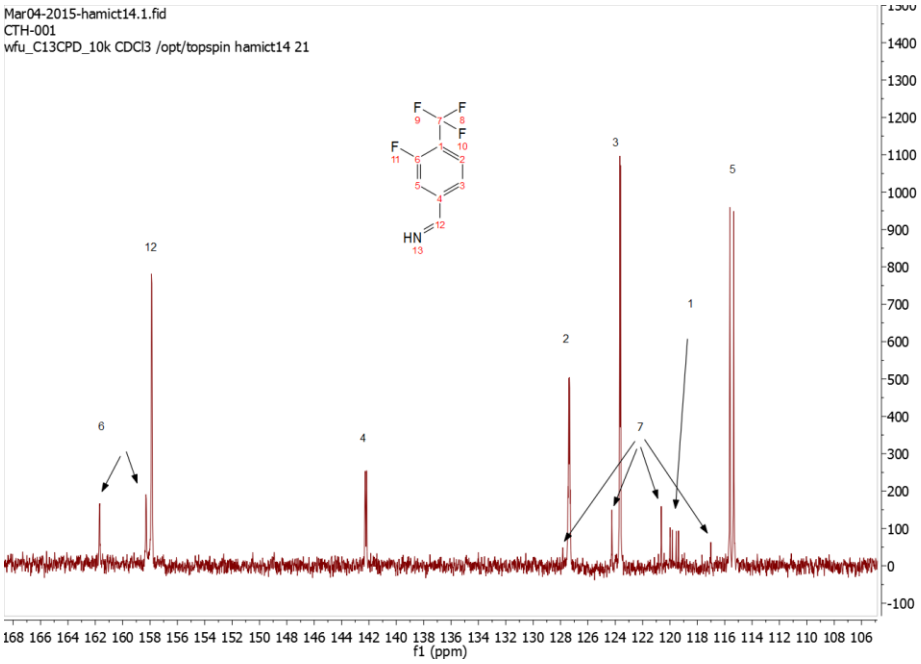

Figure 2.2. ^{13}C NMR spectrum of molecule 4.

2.2.5 Device Fabrication

The SAMs were deposited on highly-doped silicon wafers with native SiO_2 formed at their surface by either solution or vapor-based techniques. The substrates were cleaned in hot acetone, then hot isopropanol (IPA), followed by a 10-minute exposure to UV-ozone and subsequent rinse in DI water before being dried in a stream of nitrogen. The UV-ozone step serves to both remove organic contaminants and to

increase the density of hydroxyl groups on the surface. The monolayers were formed in a nitrogen (<0.1 ppm H_2O, <0.1 ppm O_2) glovebox. We found that for the long SAMs (molecules 1, 2, 3, and 4) self-assembly from a 4 mMol solution in chloroform at 30 °C provided the films of highest quality. The short SAMs (molecules 5 through 9) were amenable to deposition by vapor treatment, where the silicon wafer was placed into a sealed jar along with 11 μL of the pure SAM com- pound at 30 °C. Both methods typically took 18 to 24 hours. To remove the excess adsorbed molecules on the monolayer surface, the samples were thoroughly rinsed in chloroform followed by IPA and then immediately dried in a stream of nitrogen. The conical-tip EGaIn contact, which was used as a top soft contact for our molecular rectifiers, was created using a Micromanipulator probe holder, and a 0.5 mm diameter Micromanipulator probe tip. EGaIn was placed onto a sacrifical copper strip into which the probe tip was slowly lowered and then raised with the aid of the contact angle goniometer.

2.2.6 Surface Analysis

In order to evaluate the quality of the SAM and the best method for assembly, water contact angle measurements were conducted using a Ramé-Hart Model 200 Contact Angle Goniometer; the results are displayed in Table 2.1. A high value of the contact angle generally coincides with a higher degree of order and/or a denser film.[79] Indeed, the contact angles measured for all the SAMs were around 70°. These values agree with the measurements performed on other fluorinated SAMs deposited on SiO_2.[80] For reference, we have also measured the contact angle on untreated substrates, and that is displayed in the same figure. It can be observed that the contact

angle for bare native SiO_2 is <10°.

We employed atomic force microscopy (AFM) measurements to characterize the surface roughness prior to SAM deposition. We measured a sample of 1 cm× 1 cm and imaged a surface area of approximately 2 × 2 μm in several spots using a Nanoscope IIIA AFM (Veeco Instruments), see Figure 2.3a. This surface is of similar quality to that obtained using template stripped or flip-chip laminated metallic electrodes.[32,81] The roughness value is over an order of magnitude smaller than the height of the molecules studied here, including the shortest one, and therefore it is largely inconsequential with regard to the assembly of a film, allowing for the formation of a highly ordered film when the processing parameters are carefully tuned. A graphical illustration of this can be seen in Figure. 2.3c, where we schematically show the assembly of a long and a short molecule studied here and the respective difference in the length scales of the substrate and molecules.

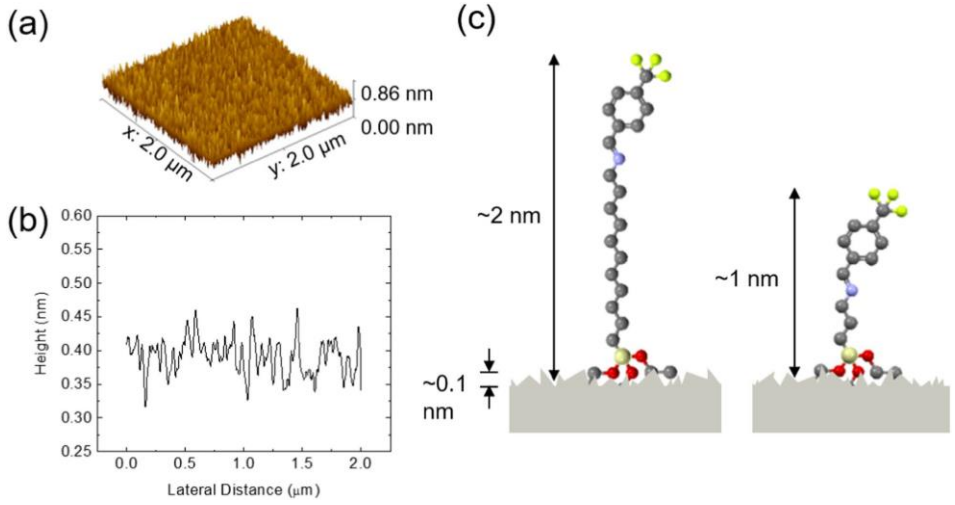

Figure 2.3. (**a**) Isometric view of a single AFM scan, (**b**) general line profile from AFM scan, and (**c**) schematic representation, to scale, of the SAM on a device substrate showing the significant difference in length for both the long (left) and short (right)

molecules compared to the surface roughness.

The work function measurements on highly doped silicon were performed using a Trek model 325 electrostatic voltmeter configured for Kelvin probe measurements and calibrated using highly-ordered pyrolytic graph- ite (HOPG) as a standard. The calculations followed from equation 2.1:

$$\varphi = -e\,(-(V\,substrate - VHOPG)) + \varphi HOPG \qquad (2.1)$$

where e is the elementary charge, $V_{substrate}$ is the measured signal from the substrate (Si with a native layer of SiO_2), V_{HOPG} is the measured signal from HOPG, and $\varphi HOPG$ is the work function of HOPG ($\varphi HOPG$ = 4.48 eV).[82] Four samples were evaluated, in at least 8 spots, and the results were consistent: we obtained a work function of φSi = 4.65 ± 0.05 eV for the highly doped Si substrates with a thin layer of native oxide on their surface.

2.2.7 Ab Initio Calculations

We performed *ab initio* calculations at the density functional theory level, using VASP.[82,83] We used the standard projector augmented wave (PAW) pseudopotentials provided by VASP along with the Perdew-Burke-Ernzerhof (PBE) exchange-correlation functional. All calculations were done with a kinetic-energy cutoff of 400 eV and an energy convergence criterion of 10−4 eV. Calculations were performed in orthorhombic unit cells with a vacuum of at least 2 nm between periodic images. All structures were relaxed until the maximum force on any atom was less than 10 meV/angstrom. Dipole moments were calculated using VASP's built-in functionality

to calculate and correct for the dipole moment in all directions (i.e. the IDIPOL and LDIPOL tags).

2.2.8 Electrical Characterization

The electrical measurements were taken on metal/SAM/metal structures using a eutectic gallium-indium (EGaIn) conical-tip top contact in which the silicon substrate was held at ground and the bias was applied to the EGaIn contact in ambient conditions. In this configuration, the forward bias condition corresponds to a positive potential applied at the fluorinated end of the molecules. The eutectic liquid metal EGaIn was utilized as a soft top-contact because its use is non-damaging, reproducible, and well-studied in this context.[20,32,40,76,84–89] A schematic of the device structure used in this study is included in Figure 2.4a. This figure, however, denotes an ideal structure of the device, while we are aware that our SAM layers may exhibit a lower degree of order, different orientation with respect to the substrate, and possible step-edges due to substrate imperfections, impurities, etc.

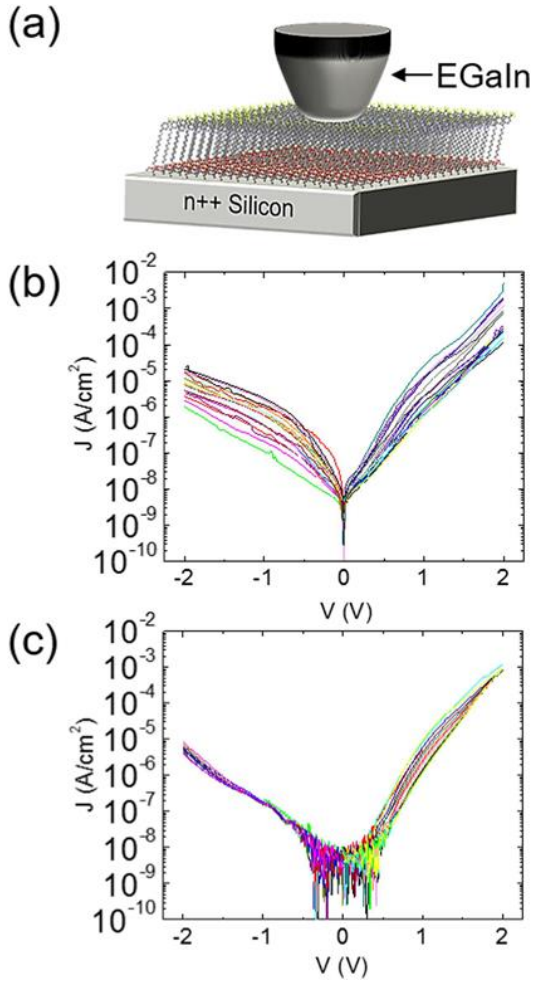

Figure 2.4. (a) Schematic of device structure showing a SAM sandwiched between the native SiO_2 bottom contact and EGaIn top contact. (b) Current density versus the applied voltage on 25 different spots in a 1 cm× 1 cm area on a film consisting of molecule 3. (c) Bias stress measurements on molecule 6 over 50 consecutive measurements in a single spot**.**

2.3 Results and Discussion

In Figure 2.4b we show the dependence of the current density (*J*) on the applied voltage (*V*) for one film of molecule 3, in 25 different spots. The relative standard deviation for these measurements is <1.4. Measurements on different spots on the films are consistent, suggesting that our SAMs are uniform. In addition, for a particular SAM

to be considered viable as a rectifier, it must be able to with- stand many repetitive measurements with minimum changes in the electrical characteristics. This could involve a variability and instability in the measured output characteristics or, in the worst-case scenario, a "breaking" of the monolayer, indicating that there is now an irreversible conductive path between the two electrodes. The good operational stability, as clearly seen in Figure 2.4c for molecule 5, where we show the results of 50 consecutive measurements, indicates that these monolayers are robust to bias stress (the relative standard deviation is less than 0.21). The difference between Figure 2.4b and 2.4c. at low voltages originates from the fact that charging effects may occur when repeated measurements are taken on the same spot on the film, causing noise and asymmetries in the measured current. We note, however, that applying higher voltages may result in irreversible damage of the SAM film. The breakdown field in these SAMs range from approximately 20 MV/cm for molecule 9 to 50 MV/cm for molecule 5.

Figure 2.5 shows typical current-voltage (*J*-*V*) characteristics for each of the 9 molecules, taken during the forward and reverse bias conditions. We measured at least 10 devices for each type of SAM, in at least 25 spots each, and obtained similar results. As expected, the magnitude of the measured current depends on the molecu- lar structure, with the long molecules generally exhibiting lower conductivities and less pronounced asymetries between the forward and reverse bias conditions.

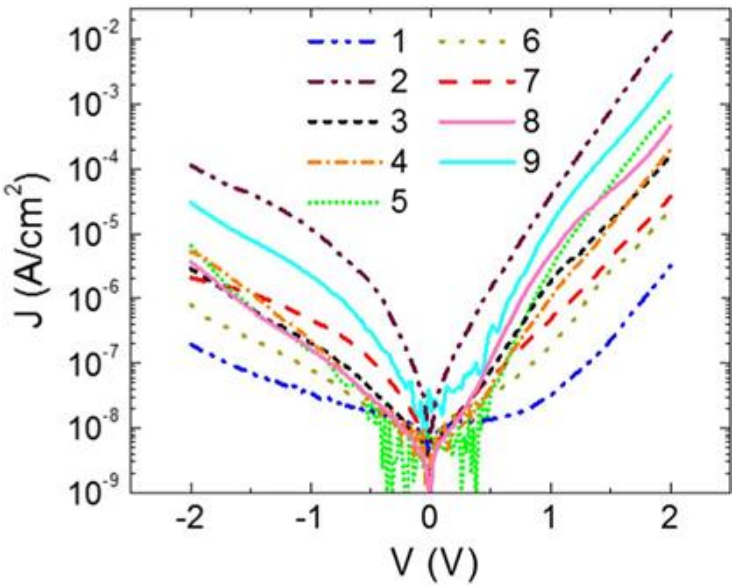

Figure 2.5. Current density versus applied voltage curves for films of molecules 1-9.

We define the rectification ratio, *R*, as the ratio between the *J* value during the forward bias measurement, (V = +2 V) and the *J* value during the reverse bias measurement, (V = −2 V):

$$R = \left|\frac{J(V = +2V)}{J(V = -2V)}\right| \qquad (2.1)$$

In Table 2.1 we list the *R* values obtained for the nine molecules. In order to relate the electrical properties with the molecular structure, we determined the electrical dipole of each molecule using DFT calculations; results are listed in Table 2.1.

Molecule	Contact Angle (°)	R	μ (D)
1	74	23 ± 8	4.50
2	72	82 ± 24	4.64
3	70	36 ± 13	2.71
4	79	80 ± 25	5.29
5	66	183 ± 41	4.42
6	74	159 ± 38	4.59
7	77	34 ± 19	2.48
8	78	192 ± 42	5.40
9	70	104 ± 10	3.21

Table 2.1. Contact angles, average rectification ratios, and dipole moments of molecules 1–9. (R values included with standard deviation).

In Figure 2.6, we plot the dependence of *R* on the molecular dipole for all the molecules investigated in this study. Results obtained for short molecules are included in red, while those for long ones are shown in grey. First, note the high value of *R* obtained for molecule 5 and 8, $R_5 = 183 \pm 41$ and $R_8 = 192 \pm 42$. These values are on par with some of the highest reported in the literature, with a thiophene-1,1-dioxide oligomer exhibiting an R of ~200, a ferrocene-alkanethiolate with an $R = 150$, and ferrocene placed on a monolayer of β-cyclodextrin demonstrating an R of 170.[38,85,90] We note, however, that larger values can also be obtained.[39,91] Nevertheless, our molecules have the additional advantage of being very low-cost since the precursors are common organic molecules, being easy to synthesize, and requiring minimal

purification steps.

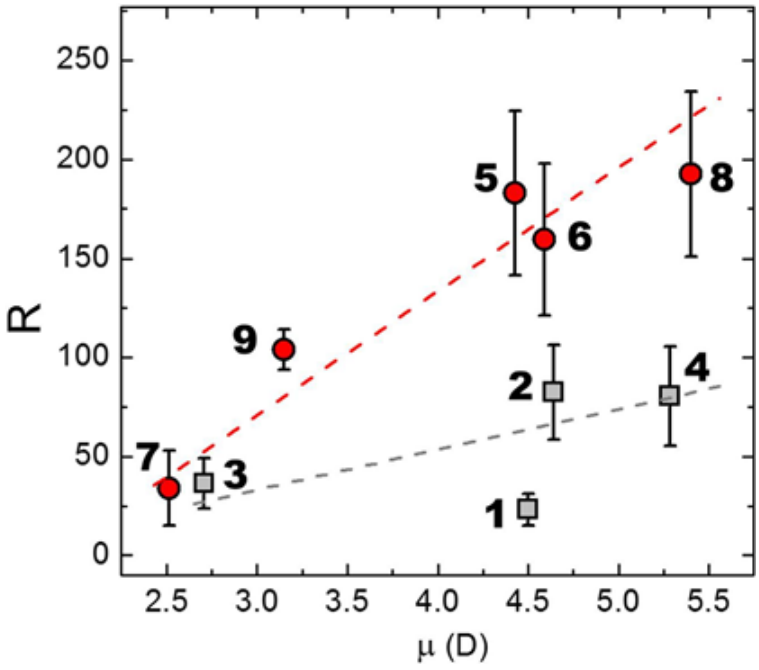

Figure 2.6. Rectification ratio vs. the dipole moment of each molecule. In red we show the results corresponding to the short molecules and in grey for the long molecules.

This figure also denotes that a stronger rectification is achieved in the case of short molecules, in agreement with previous reports.[92,93] Another key point that can be observed from Figure 2.6 is that for molecules of similar length, the rectification ratio correlates positively with the internal dipole moment of each molecule. This trend can originate from the fact that the molecular dipole creates a local electric field proportional to the magnitude of the dipole moment. This field contributes to the total net field experienced by the molecule under external bias, modifying the shape of the tunnelling barrier, and, consequently, of the current magnitude. Although a detailed interpretation of this dependence is beyond the scope of this manuscript, the results suggest that for molecules of similar length, the rectification increases with the

molecular dipole, regardless of structural details of each compound. The trend is monotonic for the case of short molecules, and we note that there is a spread in our data for the long molecules. On one hand, this may originate from variations in molecular orientation and the degree of order of the SAMs on the surfaces, which results from the competition between intermolecular interactions of the SAM molecules and molecule-substrate interactions. We attempted to characterize the ordering of the SAMs through polarized modulated-infrared reflection absorption spectroscopy (PM-IRRAS) and X-ray reflectivity measurements, both of which were unsuccessful due to the small size of the molecular layers. On the other hand, local molecular torsions and changes in the conformation were shown to significantly impact the value of the rectification ratio.[94,95] Several other factors may contribute in the observed asymmetries. First, the two contacts are not perfectly symmetric: a strong, Si-O covalent bond is established between the SAM and the bottom contact, while the top contact interacts with the SAM via a weak, van der Waals bond established between the end-group of the SAM and the Ga_2O_3 layer formed at the surface of the EGaIn electrode.[32] The strength of this bond, and therefore the rate of charge tunnelling, may vary with changing the chemistry of the SAM fluorinated functional group. In addition, these contacts have slightly different work-functions (φSi= 4.65 ± 0.05 eV, as determined from Kelvin probe measurements described above, while φEGaIn = 4.1–4.2 eV), which impact the injection of charge carriers. Second, additional dipole moments may be formed through band-bending when physical contact is established between the SAM and electrodes. Nevertheless, the dependence is clearly distinguished and this suggests that tailoring the internal molecular dipole via molecular design may be a powerful tool in controlling the rectification ratios in

molecular diodes. This result may seem to contradict that of Yoon and collaborators, who showed that the rectification behaviour of molecular diodes is independent of their molecular dipole.[70] In that study, however, the molecules had various lengths, and therefore the dependence may have been masked. Further studies, focusing on the examination of properties of different classes of compounds—including compounds with dipole moments in opposite directions—as well as studies on SAMs of different anchoring and terminal groups would clarify the generality and limitations of this method.

2.4 Conclusions

In conclusion, we have designed, synthesized, and measured nine new rectifying self-assembled monolayers of different lengths and polar terminations. We found that these fluorinated benzalkylsilane molecules exhibit high yield when incorporated in molecular diodes, coupled with robust rectification ratios ranging from 20–200, depending on their structure. In addition, they show good uniformity over large surface areas and excellent bias stress stability. We found an increase in the rectification strength with enhancing the internal molecular dipole of each molecule. Our results suggest that the electrical properties of molecular diodes can be controlled by tailoring the molecular structures of the constituent molecules. This is a significant step toward controlling the performance of molecular rectifiers through manipulating specific structure-property relationships for use in macroscopic electronics as diodes, half-wave rectifiers, AC/DC converters, or other charge-restricting elements.

CHAPTER 3

ELECTRON DONATING AND ELECTRON WITHDRAWING BENZALKYLSILANE MOLECULAR RECTIFIERS

Angela Broadnax†, Zachary Lamport‡, Andrew DelaCourt†, and Ben Sharmann‡, Mark Welker†, and Oana Jurcheschu‡

†Department of Chemistry, Wake Forest University, Winston-Salem, NC 27109,

‡Department of Physics, Wake Forest University, Winston-Salem, NC 27109

The work contained in this chapter had not been published at the time this dissertation was prepared. This chapter, including figures and schemes, was drafted by Angela Broadnax and edited by Mark Welker. The synthesis and synthetic characterization described herein was performed by Angela Broadnax and Andrew DelaCourt. Device fabrication and electrical measurements were performed by Zachary Lamport and Ben Scharmann.

3.1 Introduction

The field of molecular electronics is more appealing than ever before as silicon-based electronic devices have gotten ever-smaller and the demand for faster and cheaper processors has soared. Because single molecules constitute the smallest stable structures known, researchers have developed molecular electronics such as transistors and rectifiers to address the challenges faced with the miniaturization of electronic circuits. However, since the land mark paper by Aviram and Ratner, few molecular rectifiers have been found to compare to conventional diodes[39,96]. Most molecular rectifiers exhibit rectification ratios *R* (the current at forward bias divided by the current at reverse bias) ≤ two orders of magnitude compared to *R* values of 10^5-10^8 obtained by silicon- based diodes[37].

Some exceptions exist, though. For example, Nijhuis et al., achieved *R* values up to three and five orders of magnitude with SAMs of biferrocene sandwiched between a top EGaIn contact and bottom Ag and Pt contacts, respectively[39,96]. Although *R* values are comparable to conventional diodes, a drawback to this system is that synthesis is time intensive and requires multiple steps limiting its practicality. Additionally, the use of template stripping to achieve smooth Ag and Pt surfaces involves many steps and adds significantly to the fabrication costs of these devices[12]. Silicon substrates are an alternative to this method as silicon has a surface roughness of less than 0.1 nm without additional processing[97]. Furthermore, use of silicon substrates is advantageous because of the availability of existing knowledge and input from the very successful silicon industry.[13]

Here, we report on a series of novel benzalkylsilane molecules (Figure 3.1;

molecules 1-9) that self-assemble on silicon substrates to form high-performing molecular rectifiers. These molecules consist of a 3-carbon alkyl chain and a methanimine group connected to a benzene ring terminated with electron donating and electron withdrawing groups and were synthesized via a simple condensation reaction in high yields. We obtained *R* values up to 2635 in molecule 1, which is the highest ever obtained for molecular diodes on silicon. Based on the success of molecule 1, we also synthesized molecules 10 and 11 (Figure 3.1) for future studies on the relation between head group and molecular rectification. These molecules ease of synthesis and straight forward fabrication process makes them attractive for future applications with silicon-based electronic devices.

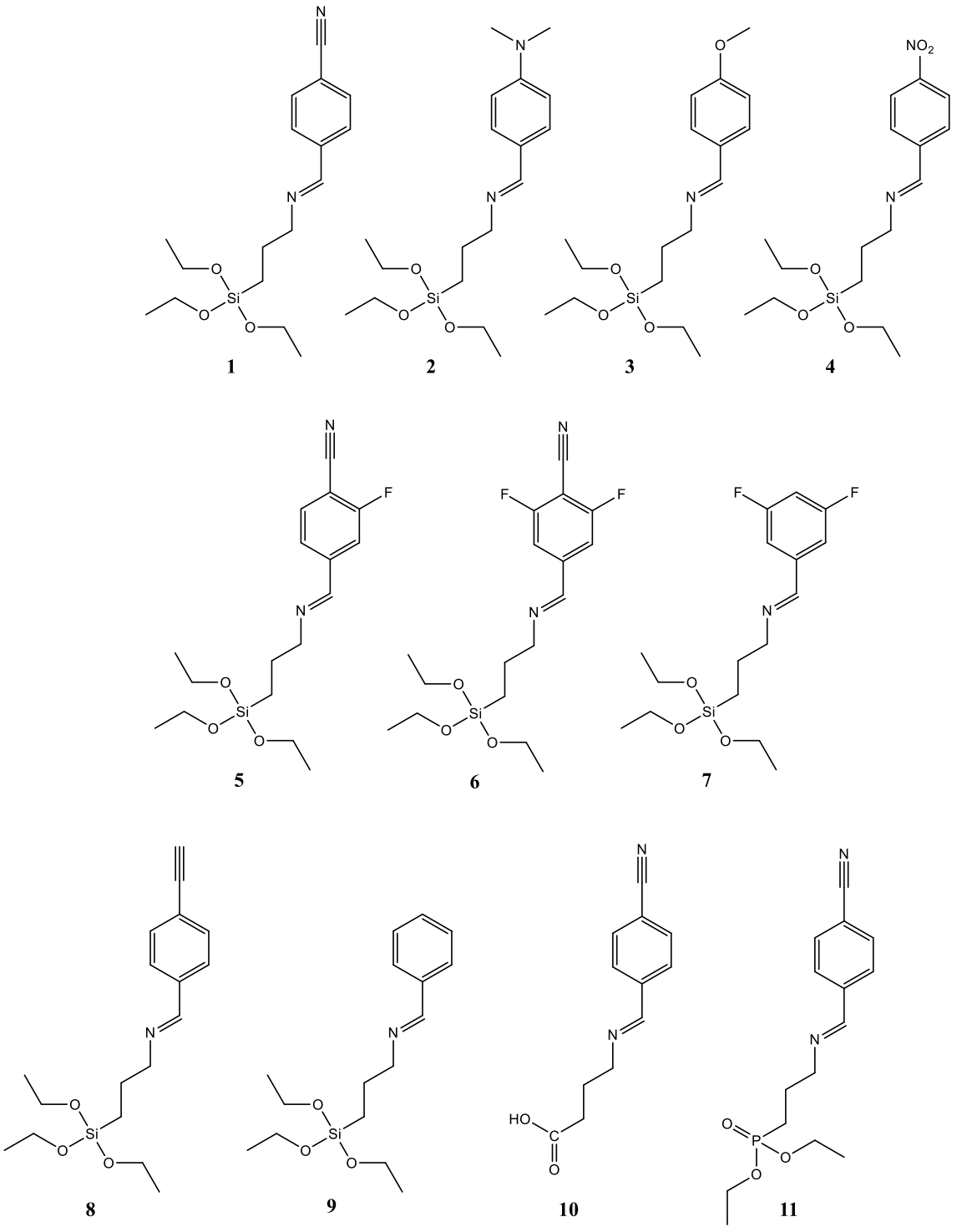

Figure 3.1. Chemical structures of molecules 1-11.

3.2 Experimental

3.2.1 Instrumental Analysis and Chemicals

The proton nuclear magnetic resonance (^{1}H NMR) spectra were obtained using a Bruker Avance 300 MHz spectrometer operating at 300.1 MHz or a Bruker Avance 500 MHz spectrometer operating at 500.1 MHz. ^{13}C NMR spectra were obtained using a Bruker Avance 300 MHz spectrometer operating at 75.5 MHz or a Bruker Avance 500 MHz spectrometer operating at 125 MHz. ^{1}H and ^{13}C NMR spectra were referenced to the residual proton or carbon signals of the respective deuterated solvents. Chemical shifts were reported in parts per million (δ) relative to tetramethylsilane (TMS) or to residual resonances of the deuterated solvents: dimethyl sulfoxide (DMSO), methanol (CD_3OD) or chloroform ($CDCl_3$). Coupling constants (J values) were reported in hertz (Hz) and spin multiplicities were indicated by the following symbols: s (singlet), d (doublet), t (triplet), q (quartet), dd (double doublet), and m (multiplet).

High-resolution mass spectrometry (HRMS) was performed at the Mass Spectrometry Facility at Wake Forest University. All reactions were carried out under an atmosphere of argon or nitrogen. Deuterated solvents were purchased from Cambridge Isotope Laboratories. Aminopropyltriethoxysilane was purchased from Aldrich Chemical Company and used as received. Anhydrous sodium sulfate was purchased from Fisher Scientific™ and used as received. 4-aminobutyric acid and all benzaldehydes came from Combi-Blocks except 4-nitrobenzaldehyde which was purchased from Acros Organics. Diethyl(3-aminopropyl)phosphonate was purchased from Beantown Chemical.

NOTE: The experimental section for molecules 1-4 and 10-11 is reported below. Molecules 5-9 were synthesized by Andrew DelaCourt and therefore the experimental section is not included.

(E)-1-(4-cyanophenyl)-N-(3-(triethoxysilyl)propyl)methanimine (**1**). Anhydrous Na_2SO_4 (3.0 g) was added to a solution of 4-formylbenzonitrile (0.131g, 1.00 mmol) in anhydrous toluene (5 mL). A solution of aminopropyltriethoxysilane (APTES) (0.243 g, 1.10 mmol) in anhydrous toluene (5 mL) was added dropwise with stirring to the resulting mixture over 5 min. After 2 h, the solution was decanted, and toluene was removed *in vacuo*. Compound **1** was isolated as a clear liquid (0.285g, 1.05mmol, 85%): ^{1}H NMR (400 MHz, Chloroform-*d*) δ 8.30 (s, 1H), 7.82 (d, *J* = 8.2 Hz, 2H), 7.70 (d, *J* = 8.2 Hz, 2H), 3.83 (q, *J* = 7.0 Hz, 6H), 3.66 (t, *J* = 6.8 Hz, 2H), 1.93 – 1.77 (m, 2H), 1.23 (t, *J* = 7.0 Hz, 9H), 0.75 – 0.61 (m, 2H). ^{13}C NMR (101 MHz, $CDCl_3$) δ 159.09, 140.16, 132.40, 128.44, 118.57, 113.73, 64.32, 58.42, 24.15, 18.31, 8.10. HRMS (ESI-ion trap) m/z: $[M + H]^+$ Calc $C_{17}H_{26}N_2O_3SiH$ 335.1791; Found 335.1783.

(E)-1-(4-dimethylaminophenyl)-N-(3-(triethoxysilyl)propyl)methanimine (2). Anhydrous Na_2SO_4 (3.0 g) was added to a solution of 4-dimethylaminobenzaldehyde (0.149 g, 1.00 mmol) in anhydrous dichloromethane (5 mL). A solution of APTES (0.221g, 1.00 mmol) in anhydrous dichloromethane (5 mL) was added dropwise with stirring to the resulting mixture over 5 min. After 23 h, the solution was decanted, and

dichloromethane was removed *in vacuo*. Compound **2** was isolated as a clear liquid (0.115 g, 0.326 mmol, 33%): ^{1}H NMR (400 MHz, Chloroform-*d*) δ 8.13 (s, 1H), 7.59 (d, *J* = 8.9 Hz, 2H), 6.69 (d, *J* = 8.9 Hz, 2H), 3.82 (q, *J* = 7.0 Hz, 6H), 3.55 (t, *J* = 7.0 Hz, 2H), 3.01 (s, 6H), 1.86 – 1.74 (m, 2H), 1.22 (t, *J* = 7.0 Hz, 9H), 0.72 – 0.62 (m, 2H). ^{13}C NMR (101 MHz, $CDCl_3$) δ 160.92, 151.94, 129.39, 124.63, 111.64, 64.36, 58.35, 40.26, 24.46, 18.32, 7.99. HRMS (ESI-ion trap) m/z: $[M + H]^+$ Calc for $C_{18}H_{32}N_2O_3SiH$ 353.2260; Found 353.2272.

(E)-1-(4-methoxyphenyl)-N-(3-(triethoxysilyl)propyl)methanimine (3). Anhydrous Na_2SO_4 (3.0 g) was added to a solution of 4-methoxybenzaldehyde (0.136 g, 1.00 mmol) in anhydrous toluene (5 mL). A solution of APTES (0.221g, 1.00 mmol) in anhydrous toluene (5 mL) was added dropwise with stirring to the resulting mixture over 5 min. After 23 h, the solution was decanted, and toluene was removed *in vacuo*. Compound **3** was isolated as a clear liquid (0.251 g, 0.739 mmol, 74%): ^{1}H NMR (400 MHz, Chloroform-*d*) δ 8.20 (s, 1H), 7.71 – 7.63 (d, *J* = 7.0 Hz, 2H), 6.99 – 6.85 (d, *J* = 7.0 Hz, 2H), 3.89 – 3.76 (m, 9H), 3.57 (t, *J* = 7.0, 1.1 Hz, 2H), 1.90 – 1.74 (m, 2H), 1.22 (t, *J* = 7.0 Hz, 9H), 0.77 – 0.58 (m, 2H). ^{13}C NMR (101 MHz, $CDCl_3$) δ 161.46, 160.33, 129.55, 129.33, 113.94, 64.27, 58.37, 55.35, 24.34, 18.31, 8.02. HRMS (ESI-ion trap) m/z: $[M + H]^+$ Calc for $C_{17}H_{29}NO_4SiH$ 340.1944; Found 340.2590.

(E)-1-(4-nitrophenyl)-N-(3-(triethoxysilyl)propyl)methanimine (4). Anhydrous Na_2SO_4 (3.0 g) was added to a solution of 4-nitrobenzaldehyde (0.151 g, 1.00 mmol) in anhydrous dichloromethane (5 mL). A solution of APTES (0.221g, 1.00 mmol) in anhydrous dichloromethane (5 mL) was added dropwise with stirring to the resulting mixture over 5 min. After 4 h, the solution was decanted, and dichloromethane was removed *in vacuo*. Compound **4** was isolated as a yellow viscous liquid (0.283 g, 0.798 mmol, 80%): ^{1}H NMR (400 MHz, Chloroform-*d*) δ 8.35 (s, 1H), 8.27 (d, *J* = 8.8 Hz, 2H), 7.89 (d, *J* = 8.8 Hz, 2H), 3.83 (q, *J* = 7.0 Hz, 6H), 3.68 (t, *J* = 6.9, 2H), 1.92 – 1.80 (m, 2H), 1.23 (t, *J* = 7.0 Hz, 10H), 0.71 – 0.65 (m, 2H). ^{13}C NMR (101 MHz, $CDCl_3$) δ 158.66, 148.93, 141.82, 128.69, 123.87, 64.42, 58.42, 24.15, 18.32, 8.13. HRMS (ESI-ion trap) m/z: $[M + H]^+$ Calc $C_{16}H_{26}N_2O_5SiH$ 355.1689; Found 355.1680.

(E)-4-((4-cyanobenzylidene)amino)butanoic acid (10).

3-aminopropylbutyric acid (0.103g, 1.00 mmol) was added to a solution of 4-formylbenzonitrile (0.131 g, 1.00 mmol) in 200 proof ethanol (6 mL). The reaction mixture was refluxed overnight (16 hours) under nitrogen. Ethanol was removed *in vacuo*. Compound **10** was isolated as a yellow solid (0.202 g, 0.934 mmol, 93%): ^{1}H NMR (400 MHz, Acetone-d6) δ 8.46 (t, J = 1.5 Hz, 1H), 8.06 – 7.93 (d, J = 8.5 Hz, 2H), 7.92 – 7.80 (d, J = 8.5 Hz, 2H), 3.71 (td, J = 6.7, 1.5 Hz, 2H), 2.42 (t, J = 7.4 Hz, 2H), 2.06 (apparent t, J = 2.2 Hz, 2H), 1.99 (p, J = 7.0 Hz, 2H). ^{13}C NMR (101 MHz, Acetone) δ 174.48, 160.61, 141.40, 133.94, 129.49, 119.15, 114.49, 60.95, 31.91, 26.91.

Diethyl (E)-(3-((4-cyanobenzylidene)amino)propyl)phosphonate (11). Diethyl (3-aminopropyl)phosphonate (0.047 g, 0.243 mmol) was added to a solution of 4-formylbenzonitrile (0.0287 g, 0.219 mmol) in 200 proof ethanol (6 mL). The reaction mixture was refluxed overnight under nitrogen. TLC revealed presence of unreacted starting material thus, added Na_2SO_4 (1.0g) and continued refluxing for 48 hours. Solution was decanted, and ethanol was removed *in vacuo*. Extracted with toluene, washing with organic layer with brine (3 X). Compound **11** was isolated as a yellow liquid (0.046 g, 0.149 mmol, 68%): ^{1}H NMR (400 MHz, Acetone-d_6) δ 8.46 (s, 1H), 7.98 (d, J = 8.6 Hz, 2H), 7.86 (d, J = 8.5 Hz, 2H), 3.71 (t, J = 6.7, 1.5 Hz, 2H), 2.42 (t, J = 7.4 Hz, 2H), 2.10 – 2.04 (m, 6H), 1.99 (p, J = 7.0 Hz, 2H). HRMS (ESI-ion trap) m/z: $[M + H]^+$ Calc $C_{15}H_{21}N_2O_3PH$ 309.1368; Found 309.1367.

3.3 Synthesis Results and Discussion

3.3.1 Reaction condition selection for molecules 1-4

We synthesized electron withdrawing and electron donating benzalkylsilanes from their corresponding benzaldehydes via a simple condensation reaction with primary amine, 3-aminopropyltriethoxysilane (APTES) as illustrated in Scheme 3.1. Both starting materials were inexpensive and commercially available. Benzaldehydes possessing strong electron withdrawing and electron donating groups by resonance were chosen to study the effect of strong dipole moments on the rectification strength. The amine was chosen because previous results (from chapter 2) revealed that amines with 3 CH_2's between the silicon and nitrogen atoms resulted in higher R values compared to amines with 11 CH_2's between both atoms.

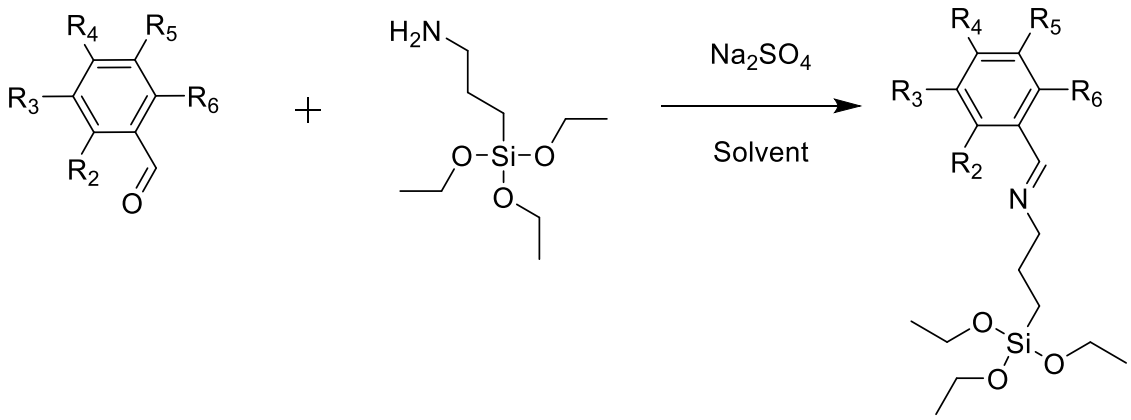

Scheme 3.1. General reaction scheme for the synthesis of molecular rectifiers 1-4.

Sodium sulfate was used to shift the equilibrium toward products by soaking up any water formed during the reaction. This resulted in high percent yields for molecules 1, 3, and 4 (74-85%). It is important to note that molecule 2 suffered from low yield due to human error, as some was lost during rotary evaporation.

It is important to take note of variations in the reaction conditions for these molecules such as the solvent used, the duration of each reaction, and the equivalents of starting material used. The two solvents utilized in these reactions were toluene and dichloromethane (DCM). Molecules 1-3 were reacted in toluene. However, when we attempted to use toluene for molecule 4, the NMR revealed a 25% excess of silane starting material in the product which we believed to be due to the limited solubility of nitrobenzaldehyde in toluene. However, after using DCM as the solvent, 15% excess of silane still remained in the product. Finally, when we changed the number of equivalents of aldehyde to silane starting material from 1:1.1 to 1:1, we achieved

molecule 4 in 80% yield. Another important procedural difference to notice is the reaction time of molecules with electron withdrawing groups compared to those with electron donating groups. Because electron withdrawing groups destabilize the aldehyde by pulling electron density away from it, it makes the aldehyde more electrophilic and hence more reactive toward nucleophilic attack from the amine. This means that reaction times should be shorter for benzaldehydes with electron withdrawing groups than with electron donating groups. As expected, molecules 1 and 4 have shorter (≤4 hours) reaction times than molecules 2 and 3 (overnight reactions).

3.3.2 Reaction condition selection for 10

Similar to molecules 1-4, molecule 10 was prepared by reacting an aldehyde and a primary amine in a condensation reaction (Scheme 3.2). Originally, toluene was used as the solvent of choice but due to the insolubility of the aminocarboxylic acid starting material, the reaction was only 50% complete after reacting for 17 hours. Ethanol proved to be a better solvent because after refluxing overnight it led to the desired product in 93% yield.

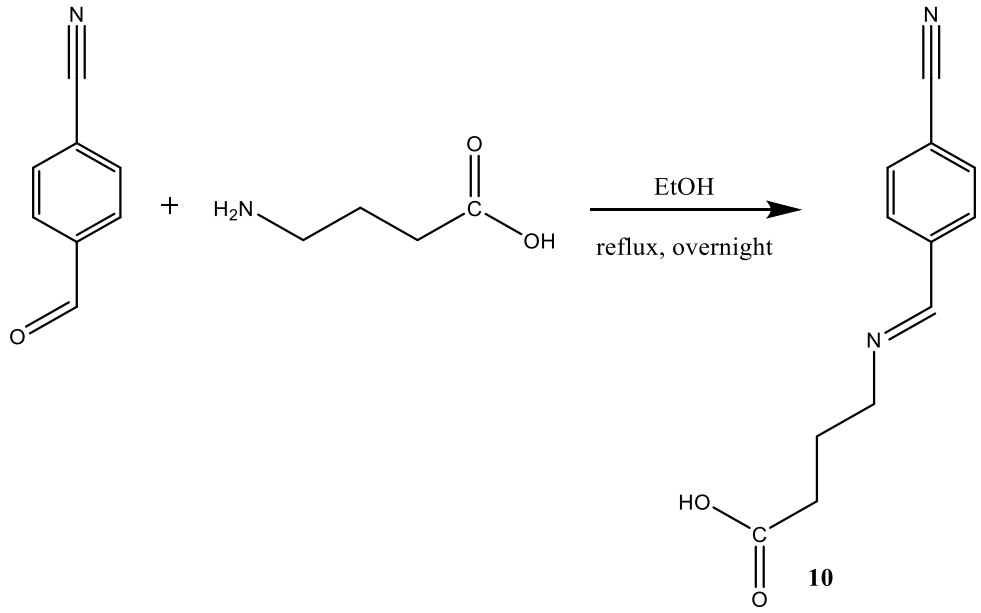

Scheme 3.2. Reaction scheme for the synthesis of molecule 10.

3.3.3 Reaction condition selection for 11

The viscous nature of 3-aminopropyldiethylphosphonate made it difficult to fill the pipet tip with the correct amount. Thus, it was added in smaller increments to ensure that we had the correct amount. The reaction was refluxed overnight under nitrogen. Due to the high flow rate of nitrogen, the solvent evaporated. Na_2SO_4 (1 g) was added to remove the water formed in reaction. The solids were re-dissolved in ethanol (12 mL) and the reaction was refluxed under nitrogen for two more days. It is important to note that careful monitoring of the reaction may result in a shorter reaction time.

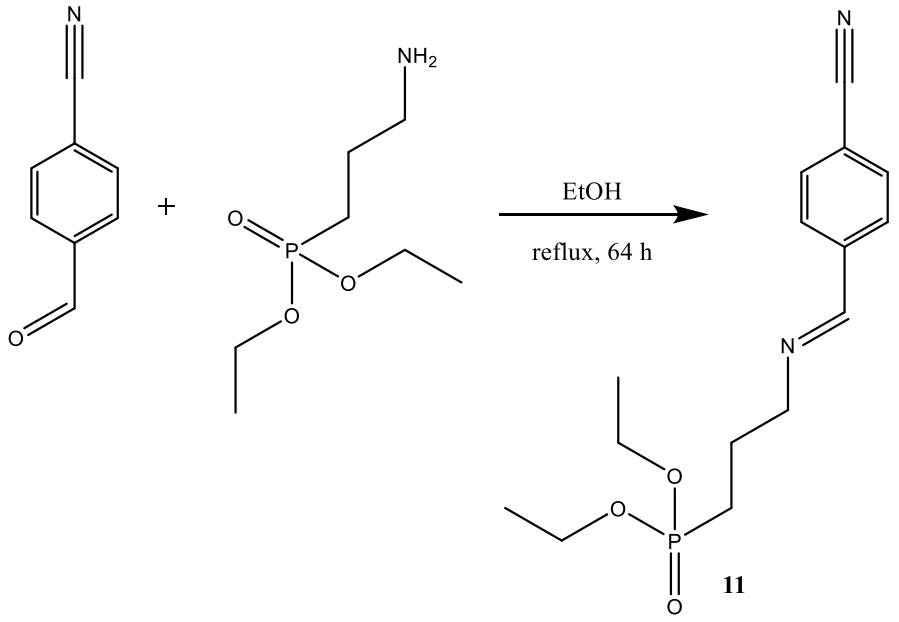

Scheme 3.3. Reaction scheme for the synthesis of molecule 11.

3.4 Device Experimental

To examine their electrical properties, the SAMs were deposited on highly-doped, natively oxidized silicon (001) wafers using solution or vapor-based deposition, as described previously. Once the SAMs were assembled, they were contacted by a top electrode cone of liquid metal EGaIn. A bias was applied to the EGaIn electrode with the silicon electrode held at ground, and the current was measured at forward and reverse bias, of up to +2 V and -2 V. The rectification ratio, which is the ratio of current density at forward bias compared to the current density at negative bias:

$$R = \left| \frac{J(V_{conducting})}{J(V_{insulating})} \right| \quad (3.1)$$

3.5 Electrical Results and Discussion

The current density at the positive bias was always higher than that at negative bias for all molecules. Thus, terminating with electron withdrawing and electron donating groups did not affect the direction of rectification. At least 70 measurements resulting from a minimum of 5 samples were characterized for each type of SAM and the results are displayed in Table 3.1, where for each molecule we list the average (R_{avg}) and maximum rectification (R_{max}) obtained for molecules 1-9. The highest rectification ratio was achieved with compound 1, R_{max} = 2635, with an average of 1683 ± 458. This *R* value to our knowledge, is the highest reported for SAMs on silicon.

Molecule	R_{max}	R_{avg}
1	2635	1683 ± 458
2	933	235 ± 162
3	590	221 ± 106
4	367	212 ± 77
5	1418	619 ± 230
6	1209	481 ± 374
7	653	264 ± 162
8	396	181 ± 100
9	676	232 ± 169

Table 3.1. Summary of electrical data for molecules 1-9.

The relationship between the structure and rectification ratio of these molecules is difficult to establish due to the complexity in isolating each factor that contributes to charge transport in a molecular junction. The rectification ratio is dependent on several factors including the molecular structure, the molecular orbital alignment and physical asymmetry of the molecule, but also the supramolecular structure of the molecular junction such as the location of the molecules relative to the electrodes and monolayer ordering/packing on the substrate. However, if we categorize these molecules, we can see how certain groups influence the rectification strength. For example, we can compare molecules 1-4 with strong electron donating and electron withdrawing functional groups and thus strong dipole moments. Despite molecules 1

and 4 both having strong electron withdrawing groups, molecule 1 gave the highest rectification ratio while molecule 4 resulted in the lowest *R* value among the 4 molecules. The difference in rectification strength may be because the nitro group in molecule 4 is bulky and can rotate about the C-N bond whereas the nitrile group in molecule 1 is small and linear and therefore would facilitate tighter monolayer packing. Comparing molecules 2 and 3, the electron donors by resonance, we see that the dimethyl amine molecule results in a higher rectification ratio than the methoxy one. These results may be attributed to the symmetry found in molecule 2 vs the asymmetry of molecule 3. Based on these results, we can say that more than just a strong dipole moment and an electron withdrawing group is required for high rectification.

We synthesized molecule 5 to further improve the rectification ratio and to understand how structure influences rectification strength. Molecule 5 contains a nitrile group in the same position as molecule 1 but a fluorine atom has been added to positively influence the rectification strength. However, this addition cuts the rectification ratio by more than half. Since the additional dipole moment and electron withdrawing group did not enhance rectification, we wanted to confirm that it was not due the geometrical asymmetry of the molecule. Comparing molecule 1 and molecules 5-7, we see that the rectification strength of these molecules is not directly proportional to the dipole moment as previously proposed for the fluorinated benzalkylsilanes[97]. Although to confirm this assumption, the molecular dipole moments should be determined using density functional theory as dipole moments can cancel out when there is symmetry in a molecule. It is important to note that the

rectification ratio for molecule 6 is higher than molecule 7 which likely means that the presence of the nitrile groups, positively impacts the rectification strength. This could mean that the nitrile group causes enhanced charge mobility because of interactions with the EGaIn electrode.

Lastly, to understand the effect of the nitrile group on the rectification strength we synthesized molecules 8 and 9. Molecule 8 is similar to molecule 1 in that it contains a linear triple bond, but it is different in that it does not contain a strong dipole moment due to the replacement of the nitrogen with a carbon atom. Because both groups are small, symmetrical, and linear, we can likely eliminate monolayer packing as a factor influencing rectification.

Molecule	R_{avg}	LUMO (eV)
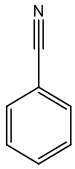 1	1683 ± 458	-4.533
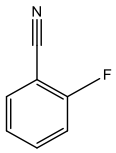 5	619 ± 230	-4.272
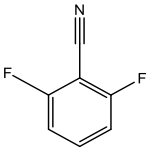 6	481 ± 374	-2.494
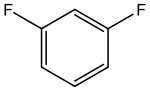 7	264 ± 162	-3.336
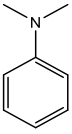 2	235 ± 162	-1.320
 9	232 ± 169	-3.581
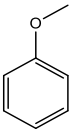 3	221 ± 106	-2.775
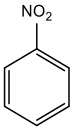 4	212 ± 77	-5.208
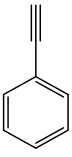 8	181 ± 100	-4.483

Table 3.2. Average R values (descending order) and LUMO energies of molecules 1-9 (calculated using Chem 3D).

It appears that dipole moment plays a crucial role in the rectification strength of molecular diodes and that the lack of a dipole moment may result in reduced rectification values. This could also be the case for molecule 9, the control molecule. However, when examining the rectification averages of molecules 2-4 and 7-9, they are all similar. Conversely, molecules 1, 5, and 6 all contain a nitrile group in the same position and have the highest *R* values. This suggests that incorporation of a nitrile group is effective at enhancing the rectification strength.

To better understand the relationship between the nitrile terminal group and the rectification strength, it may be necessary to synthesize molecules with more than one nitrile group but also to examine the HOMO and LUMO levels and how they align with the Fermi levels/work functions of the electrodes. The work function of the top EGaIn and bottom n-doped silicon electrodes are -4.3 and -4.65 eV, respectively. CHEM 3D was used to calculate the HOMO and LUMO energy levels of each molecule. Surprisingly, the HOMO energies for all molecules were very similar and between -9 and -11 eV. The LUMO energies are close to the work functions of the electrodes and thus, may be aligning with the work function of the electrodes to facilitate charge transport. Table 3.2 lists the LUMO values for molecules 1-9. There doesn't appear to be a correlation between the calculated LUMO energies and the rectification ratio. In order to elucidate the relationship between the structure and *R* value of molecules 1-9, we would need to determine their HOMO and LUMO values

of the SAMs when sandwiched between both electrodes using cyclic voltammetry.

3.6 Conclusion

In summary, we have developed molecular rectifiers with *R* values as high as 2635. This *R* value is the highest obtained for molecular rectifiers based on silicon substrates, to date. Although, the relationship between the structure and electrical function of these rectifiers is nonlinear, it appears that adding a terminal nitrile group to the benzene ring can effectively enhance the rectification strength. Elucidating the exact mechanism of rectification for these molecules by completing more in-depth studies may lead to new insights on the design of molecular rectifiers with even larger *R* values.

CHAPTER 4

FERROCENEALKYLSILANE MOLECULAR RECTIFIERS

Angela Broadnax†, Zachary Lamport‡, Ben Sharmann‡, Oana Jurcheschu‡, and Mark Welker†

†Department of Chemistry, Wake Forest University, Winston-Salem, NC 27109,

‡Department of Physics, Wake Forest University, Winston-Salem, NC 27109

This work was adapted from Angela D. Broadnax, Zachary A. Lamport, Ben Scharmann, Oana D. Jurchescu, and Mark E. Welker. *Journal of Organometallic Chemistry* 856, 23-26 (2018).

4.1 Introduction

As the length scales relevant to commercial electronics continue to shrink, great effort has been expended to explore the feasibility of devices with dimensions approaching that of a single molecule.[24–26,36,39,98,99] The molecular junctions, or molecular diodes, represent the simplest devices based on single molecule or an array of molecules sandwiched between two electrodes. In these devices the current versus voltage behavior is highly dependent on the polarity of the applied bias, i.e. they can rectify the current, similar to a pn junction. The magnitude of rectification depends on the structure and order of the monolayer, as well as the choice and quality of contacts.[28,100–103] Recently, we reported on organosilicon molecules which can be easily prepared and perform as molecular rectifiers when deposited as a self-assembled monolayer (SAM).[97] When incorporated in molecular rectifier devices, these compounds perform the same function as a diode in which current is allowed to pass through at one bias while a significantly decreased current passes at the opposite bias. We found that the rectification strength depends both on the length of the molecule and its internal molecular dipole, and we were able to reach rectifications ratios as high as 200 by controlling the molecular structure and the order of the molecular layer. In a recent paper, Nijhuis and co-workers prepared ferrocene- terminated alkanethiols with different connector groups for attaching the ferrocene to the alkanethiol and explored their rectification properties.[104] While acknowledging that it is difficult to separate electronic molecular structure changes from supramolecular structure changes on the electrical characteristics of molecular junctions, they nevertheless observed that ferrocenes substituted with electron donating groups generally assembled to provide

molecular rectifiers with rectification ratios superior to those of ferrocenes substituted by electron withdrawing groups. Similarly, ferrocene redox potentials have also been correlated with ring substituent structure in the past.[105] While these molecules present tremendous potential for molecular electronic devices, exhibiting rectification ratios as high as 200, the ferrocene precursors to the SAMs used in that work require a complex manufacturing process which involves a five to six step synthesis. In addition, a thiol anchoring group characteristic to the ferrocene SAMs utilized in these studies requires metal surfaces for self-assembly. Nevertheless, the inherent roughness of evaporated metals can be on the same length scale as the molecules forming the monolayer. To allow for a well-ordered monolayer on a metal surface, samples must be prepared by the template-stripping method, a time and cost- intensive process.[12,106] In order to make devices which are compatible with the nearly ubiquitous methods used in silicon-based technologies, we chose to use a triethoxysilane anchoring group which covalently bonds to the native oxide present on a silicon wafer. The choice of this anchoring group facilitates the use of silicon wafers, which are nearly atomically flat as grown, with no additional fabrication steps.[97] In addition, the imine and amine ferrocene molecules we propose are obtained via a one to two step synthesis, in a fast and effective process. We incorporate these compounds in molecular devices and explore how several ferrocene substituents affect the rectification behavior in these compounds.

4.2 Experimental

4.2.1 Instrumental Analysis and Chemicals

The proton nuclear magnetic resonance (1H NMR) spectra were obtained using a Bruker Avance 300 MHz spectrometer operating at 300.1 MHz or a Bruker Avance 500 MHz spectrometer operating at 500.1 MHz ^{13}C NMR spectra were obtained using a Bruker Avance 300 MHz spectrometer operating at 75.5 MHz or a Bruker Avance 500 MHz spectrometer operating at 125 MHz. ^{1}H and ^{13}C NMR spectra were referenced to the residual proton or carbon signals of the respective deuterated solvents. High-resolution mass spec- trometry was performed at the Mass Spectrometry Facility at Wake Forest University. All reactions were carried out under an atmo- sphere of argon. Aminoundecyltriethoxysilane was purchased from Gelest and used as received. Deuterated solvents were purchased from Cambridge Isotope Laboratories. Aminopropyltriethoxysilane and lithium aluminium hydride (2 M in THF) were purchased from Aldrich Chemical Company and used as received. Anhydrous so- dium sulfate was purchased from Fisher/Acros and used as received. Ferrocene carboxaldehyde was purchased from Strem Chemicals and used as received.

4.2.2 Synthesis and Characterization of Chemicals

(E)-1-(ferrocenyl)-N-(3-(triethoxysilyl)propyl)methanimine (2). Anhydrous Na_2SO_4 (2.6 g) was added to a solution of ferrocenecarboxaldehyde (0.200 g, 0.934 mmol) in anhydrous dichloromethane (4 mL). A solution of aminopropyltriethoxysilane (APTES) (0.206 g, 0.934 mmol) in anhydrous dichloromethane (4 mL) was added dropwise with stirring over 10 min. After 5 h under argon, the reddish orange mixture was filtered to

remove Na_2SO_4 and dichloromethane was removed *in vacuo*. Compound **2** was isolated as a dark red viscous liquid (0.342 g, 0.819 mmol, 88%): ^{1}H NMR (300 MHz, Chloroform-*d*) δ 8.10 (s, 1H), 4.62 (t, *J* = 1.7 Hz, 2H), 4.35 (t, *J* = 1.9 Hz, 2H), 4.18 (s, 5H), 3.83 (q, *J* = 7.0 Hz, 5H), 3.45 (t, *J* = 6.9 Hz, 2H), 1.77 (dt, *J* = 15.0, 7.0 Hz, 2H), 1.23 (t, *J* = 7.0 Hz, 9H), 0.78 – 0.58 (m, 2H).^{13}C NMR (126 MHz, $CDCl_3$) δ 160.83, 80.83, 70.22, 69.05, 68.36, 64.60, 58.37, 24.29, 18.34, 8.08. HRMS (ESI-ion trap) m/z: $[M + H]^+$ Calc $C_{20}H_{31}FeNO_3SiH$ 418.1501; Found 418.1491.

(E)-1-(ferrocenyl)-N-(3-(triethoxysilyl)propyl)methanamine (3). Lithium aluminum hydride (2M in THF) (2.56 mL, 5.12 mmol) was added dropwise to a solution of (E)- 1-(ferrocenyl)-N-(3-(triethoxysilyl)propyl)methanimine (**2**) (0.534 g, 1.28 mmol) in anhydrous THF (31 mL) at 0°C. The mixture was stirred under argon at room temperature for 12 h and then quenched with 200 proof ethanol (4.48 mL) over ice bath (0°C). The solvent was removed in vacuo. Anhydrous toluene (30 mL) was then added and the mixture was stirred at room temperature for 2 h. The oil was collected via filtration and the toluene was removed *in vacuo*. Compound **3** was isolated as a golden yellow oil (0.317 g, 0.756 mmol, 63%): ^{1}H NMR (300 MHz, Chloroform-*d*) δ 4.18 (t, *J* = 1.8 Hz, 2H), 4.12 (s, 5H), 4.09 (t, *J* = 1.8 Hz, 2H), 3.82 (q, *J* = 7.0 Hz, 6H), 3.51 (s, 2H), 2.64 (t, *J* = 7.3 Hz, 2H), 1.70 – 1.50 (m, 2H), 1.22 (t, *J* = 7.0 Hz, 9H), 0.74 – 0.55 (m, 2H). ^{13}C NMR (126 MHz, $CDCl_3$) δ 87.13, 68.41, 68.36, 67.70, 58.37, 52.44, 48.92, 23.30, 18.32, 8.00. HRMS (ESI-ion trap) m/z: $[M + H]^+$ Calc $C_{20}H_{33}FeNO_3SiH$ 420.1657; Found 420.1651.

(E)-1-(ferrocenyl)-N-(3-(triethoxysilyl)undecyl)methanimine (4). Anhydrous Na_2SO_4 (1.3 g) was added to a solution of ferrocenecarboxaldehyde (0.100 g, 0.467 mmol) in anhydrous dichloromethane (2 mL). A solution of 11-aminoundecyltriethoxysilane (AUDTES) (0.103 g, 0.467 mmol) in anhydrous dichloromethane (2 mL) was added dropwise with stirring over 10 min. After stirring under argon overnight, the red mixture was filtered to remove Na_2SO_4 and dichloromethane was removed *in vacuo*. Compound **4** was isolated as a dark red viscous liquid (0.229 g, 0.432 mmol, 93%): ^{1}H NMR (300 MHz, Chloroform-*d*) δ 8.10 (s, 1H), 4.63 (t, *J* = 1.8 Hz, 2H), 4.35 (t, *J* = 1.8 Hz, 2H), 4.18 (s, 5H), 3.81 (q, *J* = 7.0 Hz, 6H), 3.44 (t, *J* = 6.6 Hz, 2H), 1.69 – 1.57 (m, 2H), 1.27 – 1.20 (m, 25H), 0.68 – 0.54 (m, 2H). ^{13}C NMR (126 MHz, $CDCl_3$) δ 160.46, 70.24, 69.05, 68.37, 61.98, 58.28, 33.21, 30.98, 29.67, 29.63, 29.55, 29.51, 29.27, 27.38, 27.37, 22.76, 18.31, 10.39. HRMS (ESI-ion trap) m/z: $[M + H]^+$ Calc $C_{28}H_{47}FeNO_3SiH$ 530.2753; Found 530.2744.

(E)- 1-(ferrocenyl)-N-(3-(triethoxysilyl)undecyl)methanamine (5). Lithium aluminum hydride (2M in THF) (0.721 mL, 1.44 mmol) was added dropwise to a solution of (E)- 1-(ferrocenyl)-N-(3-(triethoxysilyl)undecyl)methanimine (**4**) (0.191 g, 0.361 mmol) in anhydrous THF (7 mL) at 0°C. The mixture was stirred under argon at room temperature for 48 h and then quenched with 200 proof ethanol (1.26 mL) over ice bath (0°C). The solvent was removed in vacuo. Anhydrous toluene (12 ml) was then added and the mixture was stirred at room temperature for 2 h. The oil was collected via filtration and the toluene was removed *in vacuo*. Compound **5** was isolated as a golden yellow oil (0.0310 g, 0.0583 mmol, 26%): ^{1}H NMR (500 MHz, Chloroform-*d*) δ 4.18 (t, *J* = 1.8 Hz, 2H), 4.12 (s, 5H),

4.11 – 4.09 (m, 2H), 3.81 (q, *J* = 7.0 Hz, 6H), 3.50 (s, 2H), 2.62 (t, *J* = 7.3 Hz, 2H), 1.53 – 1.44 (m, 3H), 1.30 – 1.19 (m, 25H), 0.68 – 0.58 (m, 2H).^{13}C NMR (126 MHz, $CDCl_3$) δ 87.24, 70.24, 68.44, 68.40, 68.36, 67.68, 58.29, 49.79, 49.13, 33.21, 30.15, 29.63, 29.60, 29.55, 29.27, 27.42, 22.77, 18.32, 10.40. HRMS (ESI-ion trap) m/z: $[M + H]^+$ Calc $C_{28}H_{49}FeNO_3SiH$ 532.2909; Found 532.2916.

4.2.3 Procedure for SAM Assembly

Polished, highly-doped silicon (100) wafers (1 cm by 1 cm) were cleaned in hot acetone followed by hot isopropanol (IPA) and dried in a stream of nitrogen. The wafers were then exposed to UV-ozone, which serves to remove organic contaminants as well as to in- crease the density of hydroxyl groups on the native SiO_2 surface, before rinsing with deionized water and drying in a stream of nitrogen. All SAM depositions were carried out in a nitrogen glovebox (H_2O < 0.1 ppm, O_2 < 0.1 ppm) immediately after cleaning. As com- pounds 2e5 were solid at room temperature, the monolayers were prepared using solution deposition. Substrates were placed into a 4 mMol SAM solution in room-temperature chloroform and sealed for 16-24 h and then rinsed sequentially with chloroform and IPA three times each to remove any molecules physisorbed on top of the chemisorbed monolayer.

4.2.4 Electrical characterization

Electrical measurements were carried out using a 4155C Agilent Semiconductor Parameter Analyzer with a conical-tip eutectic gallium-indium (EGaIn)

contact as a non-damaging top contact and the highly-doped silicon wafer as the bottom contact. EGaIn as a top contact is very well-studied in this application because it holds its shape while on a probe tip and deforms as a liquid upon application to a surface, greatly limiting the damage to the surface under study. The bias was applied between the EGaIn contact and the silicon wafer with the silicon held at ground. At least 40 devices were tested for each molecule. An average current-density versus voltage (*JV*) curve is shown in Figure 4.1. It can be observed that the molecular device allows the current flow in one direction (positive applied bias) and it restricts it in the opposite direction (negative bias), similar to a solid state pn junction. The inset depicts the same curve plotted on a log scale.

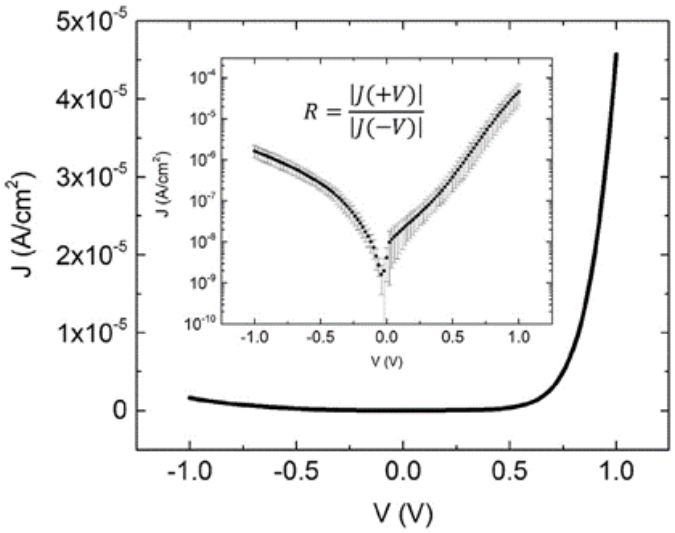

Figure 4.1. An average current-density vs. applied voltage (*JV*) curve on a linear scale, showing the diode-like operation of molecule 3 (the other compounds showed similar behavior); the inset shows the same curve using a log scale along with the definition of the rectification ratio (R).

The performance of the molecular devices is quantified by the rectification ratio (*R*), which is a measure of the selectivity of the molecular diode with respect to the

current flow direction. *R* represents the ratio between the current density measured in one direction, and the current density recorded in the opposite direction, for a given applied voltage, see the formula included as an inset to Figure 4.1. Here the top EGaIn electrode is in direct contact with the clean Si/SiO_2 sur- face. It can be observed that these measurements produce currents which are several orders of magnitude higher than that measured in our devices, confirming the fact that the very thin native SiO_2 layer does not significantly affect the current measured through the SAMs.

4.3 Results and Discussion

4.3.1 Synthesis of ferrocene complexes

Ferrocenyl imines (2, 4) were prepared in high yields by condensation of ferrocene carboxaldehyde with the appropriate aminoalkyltriethoxysilane. The moisture sensitivity of the trialkoxysilane precluded classical reductive amination approaches with aqueous work ups to the ferrocenyl amines so we instead modified a $LiAlH_4$ imine reduction procedure which had been used on aromatic imino-trialkoxysilanes previously.[107] We think the difference in the scales the two reduction reactions were typically performed on likely explains the difference in reduction yields for the short chain and long chain amines (3, 5). Stock solutions of these compounds (2-5) (Scheme 4.1) were then prepared in chloroform and stored in a refrigerator prior to use in the molecular junction experiments described below.

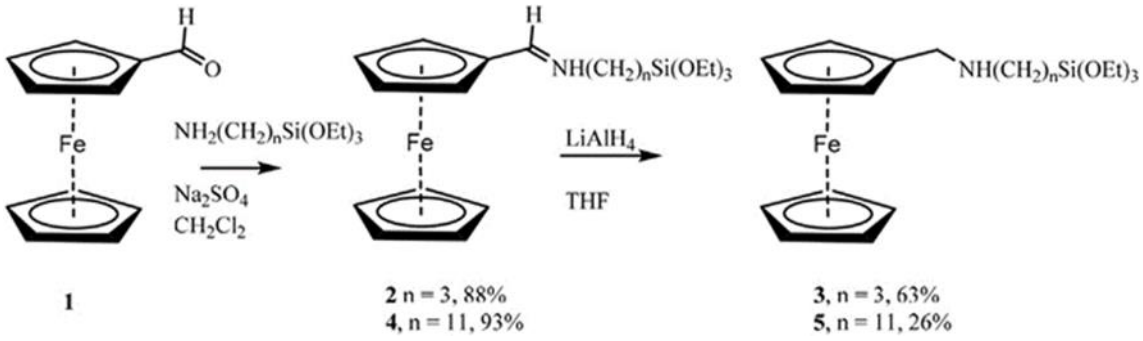

Scheme 4.1. Ferrocene Synthesis

4.3.2 Molecular Junction Characterization

To determine the efficacy of SAMs composed of compounds 2-5 as molecular rectifiers, the rectification ratio (R) was calculated from the measured JV curve, an example of which is provided in Figure 4.1, *R* was determined by dividing the current density at an applied bias of 1 V by the current density at an applied bias of -1 V. Figure 4.2 shows the results of these measurements for compounds 2-5, where each count in the histogram represents a different device formed by moving the EGaIn probe tip to another area on the substrate. Measurements on compound 2 yielded an average $R = 43.9 \pm 41.7$ with a maximum of 150, compound 3 an average of R 28.2 ± 19.4 with a maximum of 82.6, compound 4 an average of $R = 3.4 \pm 1.1$ with a maximum of 5.7, compound 5 an average of $R = 52.6 \pm 27.5$ with a maximum of 127.8. While some of these values are quite low, making them unattractive for incorporation in molecular devices, rectification strengths reaching 150 are on par with several other molecular structures that were intensely studied, and for which the fabrication is significantly more difficult. This suggests that the ferrocenealkylsilanes may offer an

attractive route for high performance molecular rectifiers upon a better under- standing of their properties in relation to their structure. Comparing to the results obtained by the Nijhuis group, our molecules which are of similar lengths (compounds 4 and 5) follow the trend that they had found in which an electron donating substituent increases the measured rectification ratio. The shorter molecules (compounds 2 and 3), however, follow the opposite trend where an electron withdrawing substituent resulted in a higher rectification ratio. This is unsurprising, given that we have previously seen that the length of the SAM in question will drastically alter the measured electrical properties, even with the same termination. These substituents presumably influence the tilt angle of the ferrocene with respect to the surface as these molecules self-assemble which largely accounts for the differences in observed rectification ratios.

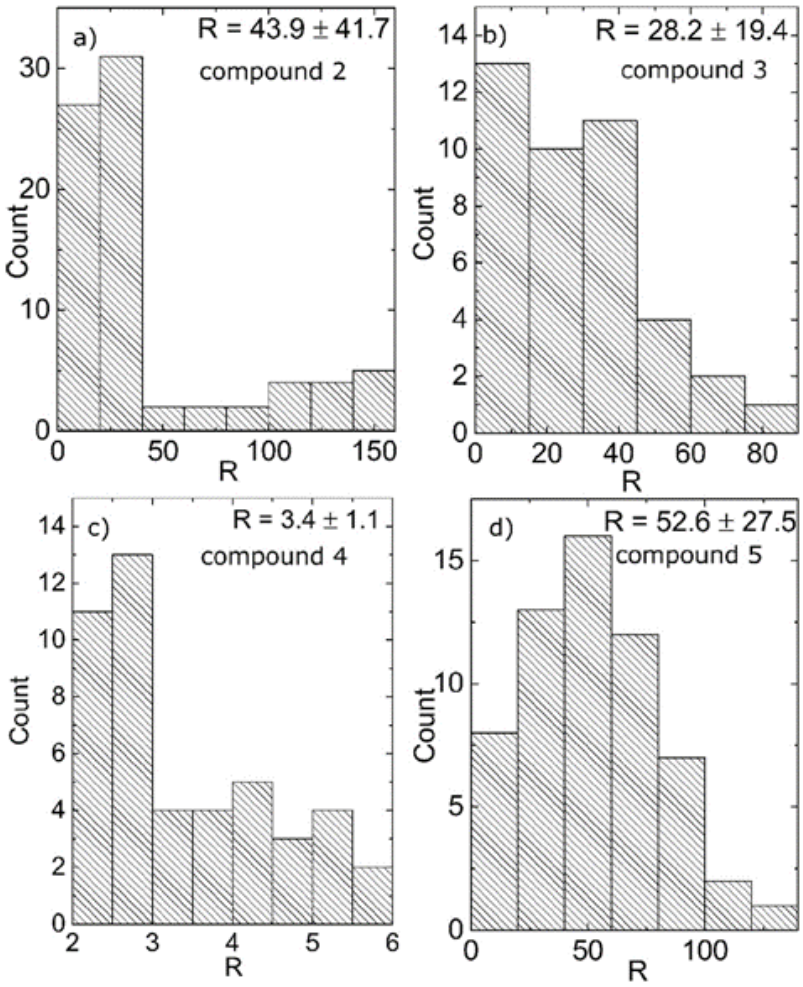

Figure 4.2. Histograms showing the measured rectification ratios of compounds 2-5.

More in depth studies are necessary in order to establish a structure-property relationship in these com- pounds and to relate the molecular structure with the orientation on the substrate (tilt angle), packing and the resulting rectification behavior. These studies will require the investigation of a larger number of compounds with different substituent groups. This knowledge will promote the development of similar molecules, which exhibit higher rectification ratios without compromising the ease of processing offered by the synthesis method described in this work.

4.4 Conclusions

In summary, we have prepared four new ferrocenyl silanes in one or two simple chemical steps. We found that these molecules can rectify the current when incorporated in molecular diode de- vices, with rectification ratios as high as 150 being recorded. Our results suggest that ferrocenyl silanes are excellent candidates for molecular electronic devices, combining the ease of processing with high performance.

CHAPTER 5

SYNTHESIS OF ANTHRACENE AND [1]BENZOTHIENO[3,2-B]BENZOTHIOPHENE -BASED IMINOSILANES

Angela Broadnax†, Zachary Lamport‡, Mark Welker†, and Oana Jurcheschu‡

†Department of Chemistry, Wake Forest University, Winston-Salem, NC 27109,
‡Department of Physics, Wake Forest University, Winston-Salem, NC 27109

The work contained in this chapter had not been published at the time this dissertation was prepared. This chapter, including figures and schemes, was drafted by Angela Broadnax and edited by Mark Welker. The synthesis and synthetic characterization described herein was performed by Angela Broadnax. Device fabrication and electrical measurements were performed by Zachary Lamport.

5.1 Introduction

Contemporary organic thin film transistors (OTFTs) suffer from low charge carrier mobility and high operating voltages. Most OTFTs operate at voltages above 40V, with mobilities lower than 1cm^2/Vs (for comparison, the carrier mobilities in silicon are above 10^2 cm^2/Vs)[41]. The operating voltage, V_{GS} is dictated by the required charge density Q in the OTFT channel, at the interface between the dielectric and the semiconductor, which, in turn, is induced by the gate-source voltage. The operating voltage and the charge density are related by the areal capacitance (ability to store charge) of the dielectric layer, C_i:

$$Q = C_i V_{GS} = \frac{\varepsilon_0 \varepsilon_r}{d} V_{GS} \tag{5.1}$$

Where ε_0 and ε_r are the permittivity of the free space and the relative permittivity of the dielectric respectively, and d is the thickness of the dielectric. Thus, a large operating voltage is not a desirable property of OTFTs and can be reduced by decreasing the dielectric thickness or employing dielectric materials with high ε_r (high permittivity). Creating high quality dielectrics thinner than 100 nm is challenging due to the inherent formation of pinholes that lead to high leakage currents[21–23].

The use of self-assembled monolayer (SAM) dielectrics has proven effective at minimizing operating voltages in OTFTs based on thermally grown organic semiconductors.[43,108–111] The monolayers form a dielectric layer of thickness ranging from 2 to about 10 nm, depending on the length and orientation of the SAM and when they are densely packed, leakage currents are extremely low (<10^{-8} A/cm^2). Their capacitance can reach 1 μF/cm^2 (estimate based on ε_r = 2.5), which is one order of magnitude higher than the value typically used in OTFTs (= 17.3 nF/cm^2), corresponding to 200 nm SiO_2

dielectric, and thus charge (Q) can be accumulated in the transistor channel at 10 times lower (VGS).

The goal of this project is to design polycyclic aromatic-based SAMs that combine the semiconductor and dielectric layers via a covalent bond to improve OTFT performance and to decrease operating voltages. Combining the semiconductor and dielectric layers of a transistor results in an ultrathin dielectric with a low dielectric constant that allows for a much higher capacitance without increasing the dielectric constant. A large dielectric constant is undesirable because it could lead to Fröhlich polarons (quasiparticles formed from a charge carrier in the semiconductor bound to the ionic polarization cloud in the dielectric) which act as scattering centers for charges moving through the saturated semiconductor. Furthermore, covalently bonded semiconductor/dielectric SAMs will result in a smoother interface for charges to pass through. On the contrary, a non-bonded semiconductor/dielectric surface will be rough (10 nm between peaks and valleys) which results in an imperfect conducting channel.

In this work, we report on the synthesis and characterization of novel anthracene and [1]Benzothieno[3,2-b]benzothiophene (BTBT)-based alkylsilanes and their precursors. The semiconductor and dielectric layers are combined via a simple and efficient aldehyde and amine condensation reaction. Self-assembled monolayers composed of these benzalkylsilanes were assembled on a highly doped silicon gate electrode. Current density measurements revealed poor charge transport from source to drain potentially due to anthracene's wide band gap and the large areal footprint of the non-linear BTBT molecule which can decrease the packing density of the SAMs.

5.2 Experimental

5.2.1 Instrumental Analysis and Chemicals

The proton nuclear magnetic resonance (^{1}H NMR) spectra were obtained using a Bruker Avance 300 MHz spectrometer operating at 300.1 MHz or a Bruker Avance 500 MHz spectrometer operating at 500.1 MHz. ^{13}C NMR spectra were obtained using a Bruker Avance 300 MHz spectrometer operating at 75.5 MHz or a Bruker Avance 500 MHz spectrometer operating at 125 MHz. ^{1}H and ^{13}C NMR spectra were referenced to the residual proton or carbon signals of the respective deuterated solvents. Chemical shifts were reported in parts per million (δ) relative to tetramethylsilane (TMS) or to residual resonances of the deuterated solvents: dimethyl sulfoxide (DMSO), methanol (CD_3OD) or chloroform ($CDCl_3$). Coupling constants (J values) were reported in hertz (Hz) and spin multiplicities were indicated by the following symbols: s (singlet), d (doublet), t (triplet), q (quartet), dd (double doublet), and m (multiplet). High-resolution mass spectrometry (HRMS) was performed at the Mass Spectrometry Facility at Wake Forest University. All reactions were carried out under an atmosphere of argon or nitrogen. Deuterated solvents were purchased from Cambridge Isotope Laboratories.

5.2.2 Synthesis and Characterization of Chemicals

(E)-1-(anthracen-9-yl)-N-(11-(triethoxysilyl)undecyl)methanimine (**3**). Anhydrous Na_2SO_4 (0.150 g) was added to a solution of 9-anthracene carboxaldehyde (0.0699 g, 0.339 mmol) in anhydrous DCM (1.5 mL). A solution of 11-aminoundecyltriethoxysilane (AUDTES) (0.113 g, 0.339 mmol) in anhydrous DCM (1 mL) was added dropwise with stirring to the resulting mixture over 5 min. After 15 h, the solution was decanted, and

DCM was removed *in vacuo*. Compound **1** was isolated as a yellow liquid (0.308 g, 0.590 mmol, 87 %): ^{1}H NMR (300 MHz, Chloroform-d) δ 9.42 (s, 1H), 8.49 (d, J = 6.3 Hz, 3H), 8.06 – 7.96 (m, 2H), 7.59 – 7.42 (m, 4H), 3.99 – 3.90 (apparent t, J = 7.0 Hz, 2H), 3.81 (q, J = 7.0 Hz, 6H), 1.92 (p, J = 7.0 Hz, 2H), 1.52 – 1.26 (m, 16H), 1.22 (t, J = 7.0 Hz, 9H), 0.72 – 0.54 (m, 2H).

Anthracene-2-carbaldehyde (**6**). 2-bromoanthracene (0.270 g, 1.05 mmol, 1 equiv.), *tert*-butyl isocyanide (474 µL, 4.20 mmol, 4 equiv.), $Pd(OAc)_2$ (0.0283 g, 12 mol %), John Phos (0.0564 g, 18 mol %), Na_2CO_3 (0.445 g, 4 equiv.), Et_3SiH (504 µL, 3 equiv.), molecular sieves, and anhydrous DMF (9.0 mL) were added to a sealed tube, and stirred at 65 °C overnight under argon. After completion of the reaction indicated by TLC, the mixture was extracted with Et_2O (3×10 mL). The combined organic phases were dried over Na_2SO_4 and concentrated under vacuum. The residue was purified by column chromatography on silica gel using 9:1 pentane: Ethyl acetate as eluent to provide the pure target product (0.110 g, 0.533 mmol, 51 %), showing identical ^{1}H and ^{13}C NMR chemical shifts to those previously reported.[112,113]

(E)-1-(anthracen-2-yl)-N-(11-(triethoxysilyl)undecyl)methanimine (**7**). Anhydrous Na_2SO_4 (0.090 g) was added to a solution of anthracene-2-carbaldehyde (**6)** (0.040 g, 0.194 mmol) in anhydrous DCM (2.5 mL). A solution of 11-aminoundecyltriethoxysilane (AUDTES) (0.0647 g, 0.194 mmol) in anhydrous DCM (0.4 mL) was added dropwise with stirring to the resulting mixture over 5 min. The solution was stirred overnight and was

decanted. Dichloromethane was removed *in vacuo* and compound **7** was isolated as a yellow solid (0.063 g, 0.121 mmol, 62%): ^{1}H NMR (300 MHz, Chloroform-*d*) δ 8.46 (d, *J* = 2.8 Hz, 2H), 8.41 (s, 1H), 8.12 (s, 1H), 8.01 (d, *J* = 5.6 Hz, 4H), 7.54 – 7.44 (m, 2H), 3.81 (q, *J* = 7.0 Hz, 6H), 3.68 (t, *J* = 7.0 Hz, 2H), 1.75 (p, *J* = 7.1 Hz, 2H), 1.37 – 1.25 (m, 16H), 1.22 (t, *J* = 7.0 Hz, 9H), 0.68 – 0.56 (m, 2H). ^{13}C NMR (75 MHz, $CDCl_3$) δ 160.81, 133.80, 132.42, 132.00, 131.21, 130.90, 128.75, 128.26, 127.31, 126.30, 125.95, 125.67, 123.00, 61.99, 58.29, 33.21, 31.06, 29.66, 29.63, 29.56, 29.51, 29.27, 27.44, 22.77, 18.31, 10.40. HRMS m/z: [M + H]+ Calc for $C_{32}H_{47}O_3NSiH$ 522.3403; Found 522.3398.

[1]Benzothieno[3,2-b]benzothiophene (**9**). Sodium hydrosulfide hydrate (1.05 g, 14.2 mmol) was added to a solution of *o*-chlorobenzaldehyde (1.00 g, 7.11 mmol) in NMP (20 mL) at 80 ºC and stirred for 1 h. Then, the mixture was heated to 180ºC and stirred for 12 h at the same temperature. The resulting mixture was poured into a saturated aqueous ammonium chloride solution (saturated, 100 mL) and cooled with an ice-bath. The resulting precipitate was collected by filtration and washed with water and acetone. The precipitate was dissolved in chloroform, and the solution was passed through a short silica gel column using 100% pentane. It was placed in the freezer to allow for crystallization, filtered, and dried in vacuo and compound **9** was isolated as a pale solid (0.304 g, 1.26 mmol, 35%), showing identical ^{1}H and ^{13}C NMR chemical shifts to those previously reported.[114]

Benzo[b]benzo[4,5]thieno[2,3-d]thiophene-1-carbaldehyde (**10**). Butyllithium (8 ml of 1.6 M solution in hexanes, 12.8 mmol) was added dropwise to a solution of **9** (400 mg, 1.67 mmol) in dry THF (48 ml) at –78 °C under argon atmosphere. The cooling bath was removed, and the mixture was stirred at room temperature for 40 min and recooled to –78 °C. N-formyl morpholine (12.6 ml, 125 mmol) was added, temperature was raised to room temperature and the mixture was stirred for 90 min. The reaction was quenched by addition of water (13 ml) and the solvent was removed under reduced pressure. The residue was dissolved in dichloromethane (80 ml), washed with water (2 × 80 ml) and brine, and dried with anhydrous sodium sulfate. The solid after evaporation was separated by column chromatography on silica gel (pentane–toluene 1:1) and compound **10** was isolated as a yellow solid (0.163 g, 0.607 mmol, 36%), showing identical ^{1}H and ^{13}C NMR chemical shifts to those previously reported.[115]

(E)-1-(benzo[b]benzo[4,5]thieno[2,3-d]thiophen-1-yl)-N-(11-(triethoxysilyl)undecyl)methanimine (**11**). Anhydrous Na_2SO_4 (0.280 g) was added to a solution of benzo[b]benzo[4,5]thieno[2,3-d]thiophene-1-carbaldehyde **(10)** (0.030 g, 0.112 mmol) in anhydrous toluene (5 mL). A solution of 11-aminoundecyltriethoxysilane (AUDTES) (0.0374 g, 0.112 mmol) in anhydrous toluene (1 mL) was added dropwise with stirring to the resulting mixture over 5 min. After refluxing for 12 h, the solution was cooled to room temperature, decanted, and solvent was removed *in vacuo*. Compound **11** was isolated as a yellow oil (0.065 g, 0.111 mmol, 99%): ^{1}H NMR (300 MHz, Chloroform-*d*) δ 8.61 (s, 1H), 8.10 – 7.75 (m, 3H), 7.68 – 7.38 (m, 4H), 3.82 (d, *J* = 7.2 Hz, 8H), 1.84 (q, *J* = 7.3 Hz, 2H), 1.46 – 1.27 (m, 16H), 1.23 (t, *J* = 13.8, 7.0 Hz, 11H), 0.63 (t, *J* = 7.9 Hz,

2H). ^{13}C NMR (75 MHz, $CDCl_3$) δ 159.25, 127.90, 125.00, 124.82, 124.50, 123.97, 123.34, 121.93, 61.54, 58.30, 33.25, 31.37, 29.70, 29.61, 29.51, 29.31, 22.77, 18.32, 10.41.

5.3 Synthesis Results and Discussion

5.3.1 Synthesis of "horizontal" anthraceneiminoundecylsilane

Although anthracene is a wide band gap organic semiconductor, we chose to synthesize its analogue, molecule 3 (Scheme 5.1), because the aldehyde starting material (9-anthracene carbaldehyde) is inexpensive and commercially available. Additionally, anthracene has more organic solubility than the more extended polycyclic aromatic hydrocarbons (i.e., pentacene). We chose 11-aminoundecyltriethoxysilane to react with the aldehyde because it is commercially available and long alkyl chains have shown to positively influence the ordering and packing density in SAMs due to van der Waals interactions between adjacent chains. Lower leakage current is generally a consequence of the high extent of intermolecular interactions in OTFTs.

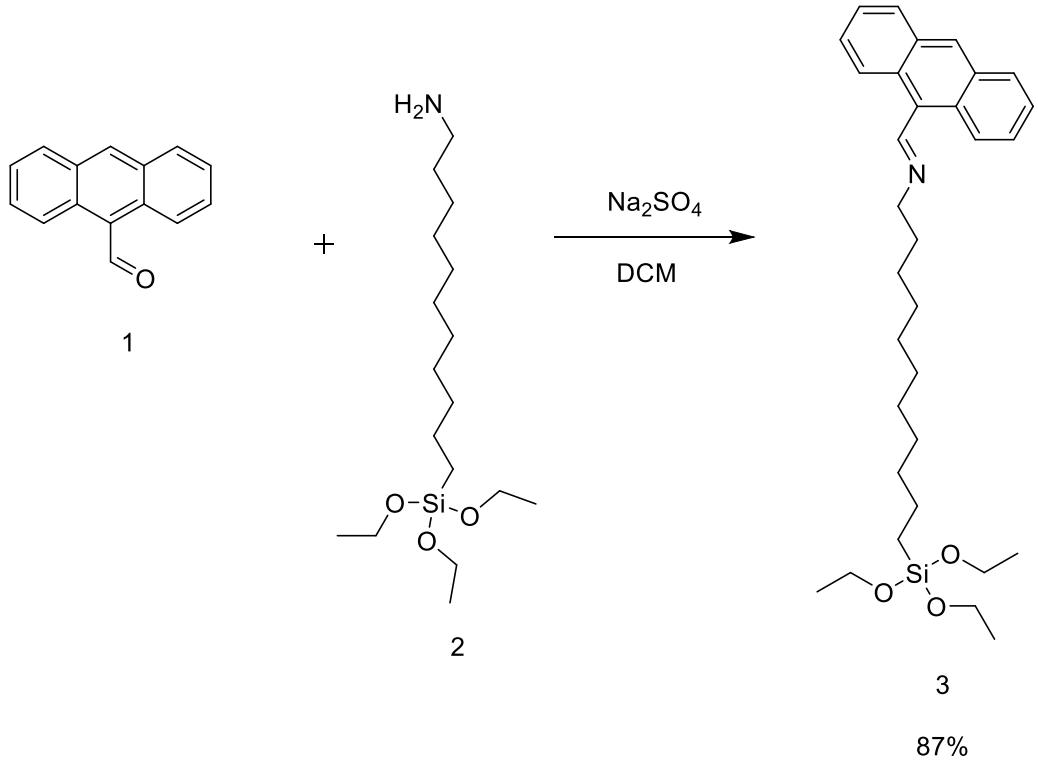

Scheme 5.1. Synthesis of "horizontal" anthraceneiminoundecylsilane, 3.

5.3.2 Synthesis of "vertical" anthraceneiminoundecylsilane

2-anthracene carbaldehyde (6) was used to synthesize the "vertical" anthraceneundecylsilane analogue. However, because the aldehyde was not commercially available, it was prepared via a palladium catalyzed formylation reaction using 2-bromoanthracene and formylating agent tert-butyl isocyanide. The following palladium catalyzed reaction illustrated in scheme 5.2 led to a moderate (51%) yield of 2-anthracene carbaldehyde:

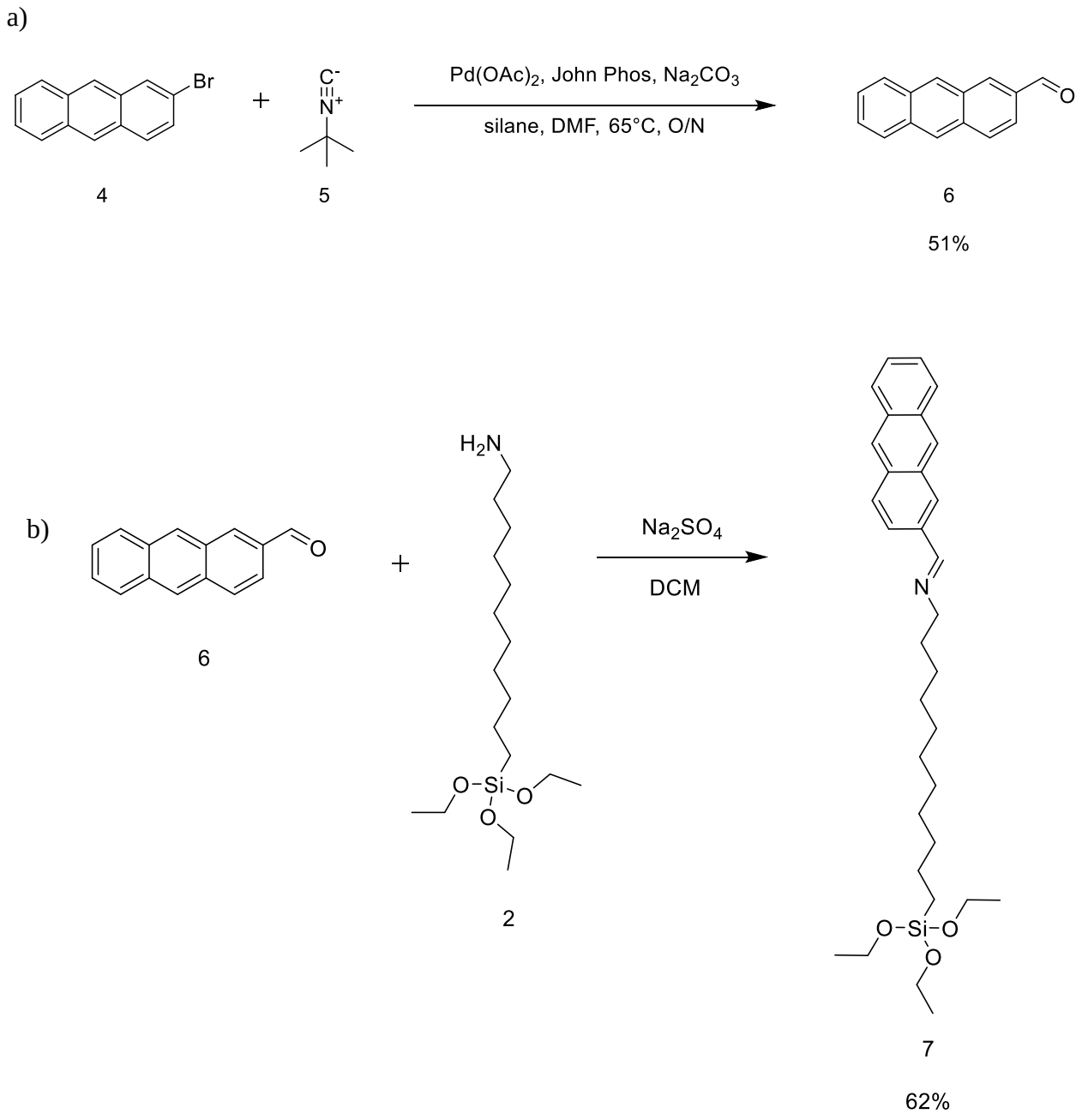

Scheme 5.2. a) Synthesis of 2-anthracene carbaldehyde, 6 and b) Synthesis of "vertical" anthraceneiminoundecylsilane, 7.

5.3.3 Synthesis of BTBT

We chose the BTBT core for our work with organic semiconductors due to its ability to promote high charge mobilities in OTFTs[54]. Although BTBT is commercially available, 1 G of reagent costs ~$400. Thus, BTBT was synthesized in one step using molecule 8, 2 equivalents of $NaSH \cdot XH_2O$, and N-methyl pyrrolidone (NMP) as the solvent. We achieved the cyclized product with a yield of 36% which is close to the reported yield of 39%, one of the highest reported yields for the synthesis of BTBT. Despite the low yield, this reaction is advantageous because commercially available orthochlorobenzaldehyde (8) can be directly converted into BTBT in a one-step reaction and the reaction can be readily scaled up to give 30 G of product as reported by Saito et al.

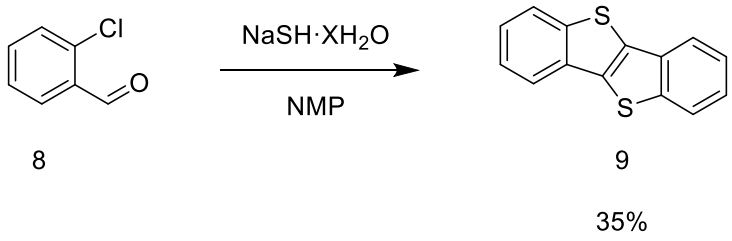

8 9

35%

Scheme 5.3. Synthesis of BTBT, 9.

5.3.4 Synthesis of "Horizontal" BTBT aldehyde

Formylation of BTBT was carried out with butyl lithium and formylating agent N-formyl morpholine to give the major product 10 in 36% yield. It is important to note here

that initially we used DMF as the formylating reagent, but the highest yield obtained was only ~19%. Upon switching to N-formyl morpholine, the product yield almost doubled.

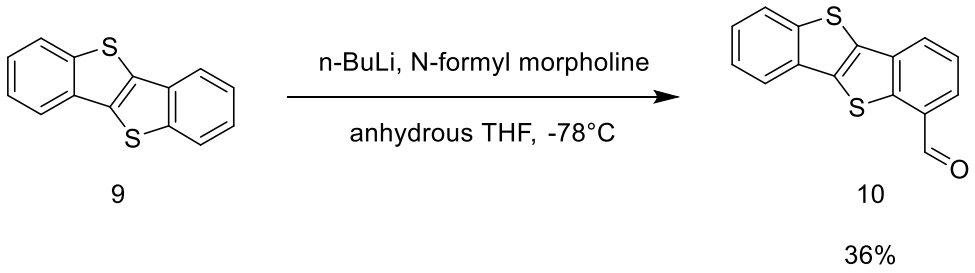

9 10

36%

Scheme 5.4. Synthesis of BTBT-1-carbaldehyde, 10.

5.3.5 Synthesis of "Horizontal" BTBT-iminoundecylsilane

Finally, the corresponding imine of BTBT-1-carbaldehyde was synthesized in a quantitative yield.

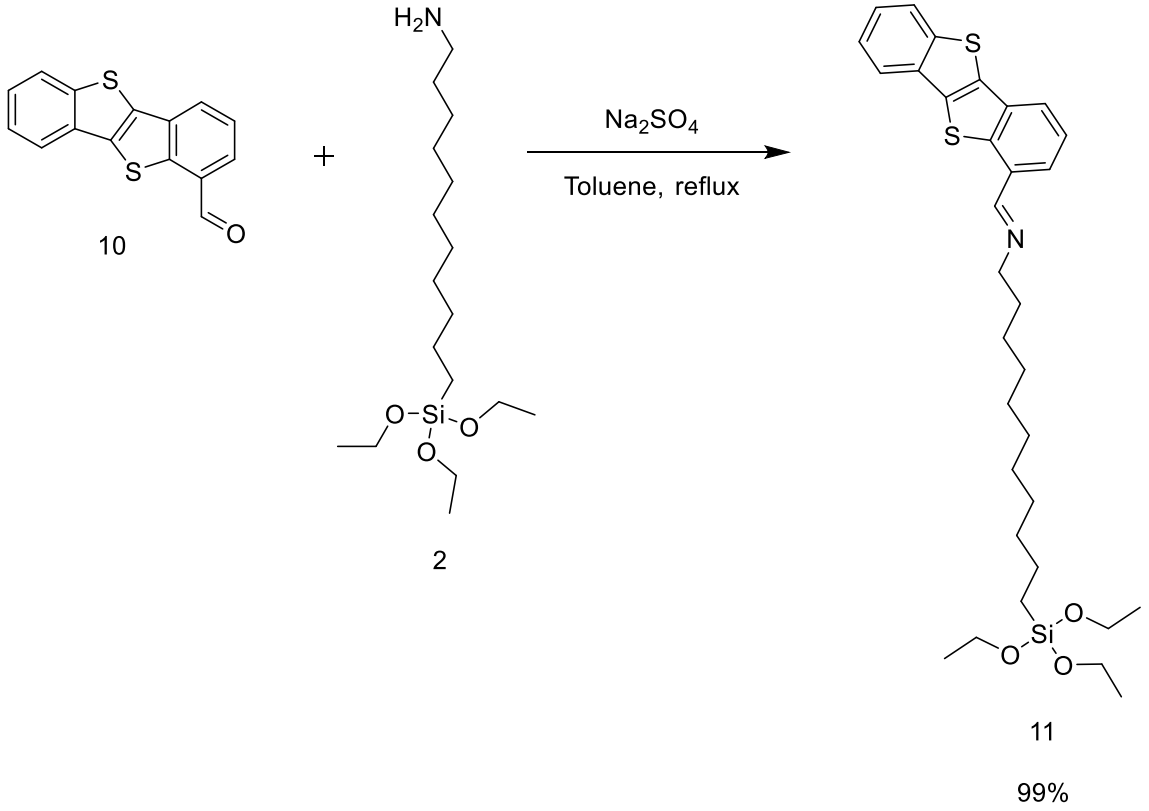

Scheme 5.5. Synthesis of BTBT-iminoundecylsilane, 11.

5.4 Device Fabrication Results and Discussion

The SAMs were assembled from a chloroform solution and contact angle measurements were used to verify the best procedure for assembly. Attempts of evaporating contacts of both gold and silver through a shadow mask, as well as a spray-coating of PEDOT:PSS (a conductive macromolecular salt) in each case resulted in monolayer short circuiting. The poor results are believed to be due to the formation of conductive filaments through the monolayer which arises from the low film density of the

"horizontal" BTBT alkylsilanes. The "horizontal" shape of the molecule creates a larger footprint on the surface which lowers the number of molecules that can fit in a given space.

5.5 Conclusions

We have synthesized anthracene and BTBT-based imino undecyltriethoxysilanes in quantitative yields from their aldehyde and amino triethoxysilane precursors. Self-assembled monolayers of the molecules were assembled on an insulating surface consisting of silicon oxide and contacted by top electrodes to make an OTFT. However, the electrical measurements shorted through the monolayer possibly due to the formation of conductive filaments through the monolayer. We hope to overcome this challenge by synthesizing molecules with a small footprint per molecule (i.e., "vertical" BTBT imino undecyltriethoxy) on the surface. This design will most likely result in increased packing density in the monolayer which would lead to enhanced charge transport.

References

1. Gordon E. Moore. Cramming more components onto integrated circuits. *Electronics* **38,** (1965).

2. Sekulic Dalibor, Z. M. A Model of the Molecular Rectifying Diode Type Aviram-Ratner. *Electronics* 23–26 (2010).

3. Hussain, S. A. & Bhattacharjee, D. Langmuir-Blodgett Films a unique tool for molecular electronics. *Mod. Phys. Lett. B* **23,** 1–9 (2009).

4. Roberts, G. G. (Gareth G. *Langmuir-Blodgett films*. (Plenum Press, 1990).

5. Metzger, R. M. Unimolecular rectifiers: Present status. *Chem. Phys.* **326,** 176–187 (2006).

6. Osvaldo, N. & Oliveira, J. Langmuir-Blodgett Films - Properties and Possible Applications. *Brazilian J. Phys.* **22,** 60–69 (1992).

7. Tredgold, R. H. The physics of Langmuir-Blodgett films. *Reports Prog. Phys.* **50,** 1609–1656 (1987).

8. Cui, X. D. *et al.* Reproducible measurement of single-molecule conductivity. *Science* **294,** 571–4 (2001).

9. Schreiber, F. Structure and growth of self-assembling monolayers. *Prog. Surf. Sci.* **65,** 151–257 (2000).

10. Aswal, D. K., Lenfant, S., Guerin, D., Yakhmi, J. V. & Vuillaume, D. Self assembled monolayers on silicon for molecular electronics. *Analytica Chimica Acta* **568,** 84–108 (2006).

11. Schwartz, D. K. Mechanisms and Kinetics of Self-Assembled Monolayer Formation. *Annu. Rev. Phys. Chem.* **52,** 107–137 (2001).

12. Weiss, E. A. *et al.* Si/SiO2-templated formation of ultraflat metal surfaces on glass, polymer, and solder supports: Their use as substrates for self-assembled monolayers. *Langmuir* **23,** 9686–9694 (2007).

13. Aswal, D. K., Lenfant, S., Guerin, D., Yakhmi, J. V. & Vuillaume, D. Self assembled monolayers on silicon for molecular electronics. *Anal. Chim. Acta* **568,** 84–108 (2006).

14. Aswal, D. K., Lenfant, S., Guerin, D., Yakhmi, J. V. & Vuillaume, D. A Tunnel Current in Self-Assembled Monolayers of 3-Mercaptopropyltrimethoxysilane. *Small* **1,** 725–729 (2005).

15. Bain, C. D. *et al.* Formation of monolayer films by the spontaneous assembly of organic thiols from solution onto gold. *J. Am. Chem. Soc.* **111,** 321–335 (1989).

16. Smith, R. K., Lewis, P. A. & Weiss, P. S. Patterning self-assembled monolayers. *Prog. Surf. Sci.* **75,** 1–68 (2004).

17. Lu, X. *et al.* Electron transport through a self-assembled monolayer of thiol-end-functionalized tetraphenylporphines and metal tetraphenylporphines. *Langmuir* **22,** 3035–3039 (2006).

18. Zhang, G.-P., Wang, S., Wei, M.-Z., Hu, G.-C. & Wang, C.-K. Tuning the Direction of Rectification by Adjusting the Location of the Bipyridyl Group in Alkanethiolate Molecular Diodes. *J. Phys. Chem. C* **121,** 7643–7648 (2017).

19. Yazdani, A., Eigler, D. M. & Lang, N. D. Off-resonance conduction through atomic wires. *Science (80-.).* **272,** 1921–1924 (1996).

20. Chiechi, R. C., Weiss, E. A., Dickey, M. D. & Whitesides, G. M. Eutectic Gallium–Indium (EGaIn): A Moldable Liquid Metal for Electrical Characterization of Self-Assembled Monolayers. *Angew. Chemie Int. Ed.* **47,** 142–144 (2008).

21. Cademartiri, L. *et al.* Electrical Resistance of Ag^{TS}–$S(CH_2)_{n-1}CH_3$//Ga_2O_3/EGaIn Tunneling Junctions. *J. Phys. Chem. C* **116,** 10848–10860 (2012).

22. Waidelich, D. L. Rectifier. *AccessScience* (2014). doi:10.1036/1097-8542.575800

23. Molecular Diode Studies Based on a Highly Sensitive Molecular Measurement Technique. *Sensors* **17,** 956 (2017).

24. Aviram, A. & Ratner, M. A. Molecular rectifiers. *Chem. Phys. Lett.* **29,** 277–283 (1974).

25. Batra, A. *et al.* Tuning rectification in single-molecular diodes. *Nano Lett.* **13,** 6233–6237 (2013).

26. Kornilovitch, P. E., Bratkovsky, A. M. & Stanley Williams, R. Current rectification by molecules with asymmetric tunneling barriers. *Phys. Rev. B* **66,** 165436 (2002).

27. Wang, L. Ferrocene-based molecular electronics and nanomanufacturing of Pd nanowires. (2007).

28. Van Dyck, C. & Ratner, M. A. Molecular Rectifiers: A New Design Based on Asymmetric Anchoring Moieties. *Nano Lett.* **15,** 1577–1584 (2015).

29. Xiang, D., Wang, X., Jia, C., Lee, T. & Guo, X. Molecular-Scale Electronics: From

Concept to Function. *Chemical Reviews* **116,** 4318–4440 (2016).

30. Metzger, R. M. *et al.* Unimolecular electrical rectification in hexadecylquinolinium tricyanoquinodimethanide. *J. Am. Chem. Soc.* **119,** 10455–10466 (1997).

31. Ashwell, G. J., Urasinska, B. & Tyrrell, W. D. Molecules that mimic Schottky diodes. *Phys. Chem. Chem. Phys.* **8,** 3314–3319 (2006).

32. Nijhuis, C. A., Reus, W. F. & Whitesides, G. M. Molecular Rectification in Metal−SAM−Metal Oxide−Metal Junctions. *J. Am. Chem. Soc.* **131,** 17814–17827 (2009).

33. McCreery, R. *et al.* Molecular Rectification and Conductance Switching in Carbon-Based Molecular Junctions by Structural Rearrangement Accompanying Electron Injection. *J. Am. Chem. Soc.* **125,** 10748–10758 (2003).

34. Liu, R., Ke, S.-H., Yang, W. & Baranger, H. U. Organometallic molecular rectification. *J. Chem. Phys.* **124,** 024718 (2006).

35. De Boer, B. *et al.* Metallic contact formation for molecular electronics: Interactions between vapor-deposited metals and self-assembled monolayers of conjugated mono- and dithiols. *Langmuir* **20,** 1539–1542 (2004).

36. Lenfant, S., Krzeminski, C., Delerue, C., Allan, G. & Vuillaume, D. Molecular rectifying diodes from self-assembly on silicon. *Nano Lett.* **3,** 741–746 (2003).

37. Nijhuis, C. A., Reus, W. F. & Whitesides, G. M. Molecular rectification in metal-SAM-metal oxide-metal junctions. *J. Am. Chem. Soc.* **131,** 17814–17827 (2009).

38. Nerngchamnong, N. *et al.* The role of van der Waals forces in the performance of

molecular diodes. *Nat. Nanotechnol.* **8,** 113–8 (2013).

39. Yuan, L., Breuer, R., Jiang, L., Schmittel, M. & Nijhuis, C. A. A Molecular Diode with a Statistically Robust Rectification Ratio of Three Orders of Magnitude. *Nano Lett.* **15,** 5506–5512 (2015).

40. Yoon, H. J. *et al.* Rectification in tunneling junctions: 2,2'-bipyridyl-terminated n -alkanethiolates. *J. Am. Chem. Soc.* **136,** 17155–17162 (2014).

41. Klauk, H. Organic thin-film transistors. *Chem. Soc. Rev.* **39,** 2643–2666 (2010).

42. Cho, J. H. *et al.* Printable ion-gel gate dielectrics for low-voltage polymer thin-film transistors on plastic. *Nat. Mater.* **7,** 900–906 (2008).

43. Facchetti, A., Yoon, M.-H. & Marks, T. J. Gate Dielectrics for Organic Field-Effect Transistors: New Opportunities for Organic Electronics. *Adv. Mater.* **17,** 1705–1725 (2005).

44. Cramer, T. *et al.* Water-gated organic field effect transistors – opportunities for biochemical sensing and extracellular signal transduction. *J. Mater. Chem. B* **1,** 3728–3741 (2013).

45. *Organic Thin Film Transistor Integration: A Hybrid Approach*. (John Wiley and Sons, 2011).

46. Anthony, J. E. Functionalized acenes and heteroacenes for organic electronics. *Chem. Rev.* **106,** 5028–5048 (2006).

47. Takimiya, K., Osaka, I., Mori, T. & Nakano, M. Organic Semiconductors Based on [1]Benzothieno[3,2- *b*][1]benzothiophene Substructure. *Acc. Chem. Res.* **47,** 1493–

1502 (2014).

48. Ebata, H. *et al.* Highly soluble [1]benzothieno[3,2-b]benzothiophene (BTBT) derivatives for high-performance, solution-processed organic field-effect transistors. *J. Am. Chem. Soc.* **129,** 15732–15733 (2007).

49. Minemawari, H. *et al.* Inkjet printing of single-crystal films. *Nature* **475,** 364–367 (2011).

50. Yuan, Y. *et al.* Ultra-high mobility transparent organic thin film transistors grown by an off-centre spin-coating method. *Nat. Commun.* **5,** 3005 (2014).

51. Podzorov, V. π-Electron systems: Building molecules for a function. *Nat. Mater.* **9,** 616–617 (2010).

52. Jackson, T. N. Organic Semiconductors: Beyond Moore's Law. *Nat. Mater.* **4,** 581–582 (2005).

53. Gundlach, D. J. Organic electronics: Low power, high impact. *Nat. Mater.* **6,** 173–174 (2007).

54. Zirkl, M. *et al.* Low-Voltage Organic Thin-Film Transistors with High-k Nanocomposite Gate Dielectrics for Flexible Electronics and Optothermal Sensors. *Adv. Mater.* **19,** 2241–2245 (2007).

55. Majewski, L. A., Schroeder, R. & Grell, M. One Volt Organic Transistor. *Adv. Mater.* **17,** 192–196 (2005).

56. Yoon, W.-J. & Berger, P. R. Atomic layer deposited HfO2 gate dielectrics for low-voltage operating, high-performance poly-(3-hexythiophene) organic thin-film

transistors. *Org. Electron.* **11,** 1719–1722 (2010).

57. Naber, R. C. G. *et al.* High-performance solution-processed polymer ferroelectric field-effect transistors. *Nat. Mater.* **4,** 243–248 (2005).

58. Schroeder, R., Majewski, L. A. & Grell, M. All-Organic Permanent Memory Transistor Using an Amorphous, Spin-Cast Ferroelectric-like Gate Insulator. *Adv. Mater.* **16,** 633–636 (2004).

59. Ukah, N. B., Granstrom, J., Gari, R. R. S., King, G. M. & Guha, S. Low-operating voltage and stable organic field-effect transistors with poly (methyl methacrylate) gate dielectric solution deposited from a high dipole moment solvent. *Appl. Phys. Lett.* **99,** 243302 (2011).

60. Hulea, I. N. *et al.* Tunable Fröhlich polarons in organic single-crystal transistors. *Nat. Mater.* **5,** 982–986 (2006).

61. Collier, C. P. *et al.* Electronically configurable molecular-based logic gates. *Science* **285,** 391–4 (1999).

62. Reed, M. A., Chen, J., Rawlett, A. M., Price, D. W. & Tour, J. M. Molecular random access memory cell. *Appl. Phys. Lett.* **78,** 3735–3737 (2001).

63. Green, J. E. *et al.* A 160-kilobit molecular electronic memory patterned at 1011 bits per square centimetre. *Nature* **445,** 414–417 (2007).

64. Rascón-Ramos, H., Artés, J. M., Li, Y. & Hihath, J. Binding configurations and intramolecular strain in single-molecule devices. *Nat. Mater.* **14,** 517–522 (2015).

65. Haedler, A. T. *et al.* Long-range energy transport in single supramolecular

nanofibres at room temperature. *Nature* **523,** 196–199 (2015).

66. Lörtscher, E. Wiring molecules into circuits. *Nat. Nanotechnol.* **8,** 381–384 (2013).

67. Metzger, R. M. Unimolecular Electronics. *Chem. Rev.* **115,** 5056–5115 (2015).

68. Akkerman, H. B. & de Boer, B. Electrical conduction through single molecules and self-assembled monolayers. *J. Phys. Condens. Matter* **20,** 013001 (2008).

69. Metzger, R. M. Unimolecular electrical rectifiers. *Chem. Rev.* **103,** 3803–3834 (2003).

70. Yoon, H. J., Bowers, C. M., Baghbanzadeh, M. & Whitesides, G. M. The Rate of Charge Tunneling Is Insensitive to Polar Terminal Groups in Self-Assembled Monolayers in $Ag^{TS}S(CH_2)_n M(CH_2)_m T//Ga_2O_3$/EGaIn Junctions. *J. Am. Chem. Soc.* **136,** 16–19 (2014).

71. Kornilovitch, P. E., Bratkovsky, A. M. & Williams, R. S. Current rectification by molecules with asymmetric tunneling barriers. (2002). doi:10.1103/PhysRevB.66.165436

72. Akkerman, H. B., Blom, P. W. M., de Leeuw, D. M. & de Boer, B. Towards molecular electronics with large-area molecular junctions. *Nature* **441,** 69–72 (2006).

73. Ashwell, G. J., Tyrrell, W. D. & Whittam, A. J. Molecular rectification: Self-assembled monolayers in which donor-(π-bridge)-acceptor moieties are centrally located and symmetrically coupled to both gold electrodes. *J. Am. Chem. Soc.* **126,** 7102–7110 (2004).

74. Elbing, M. *et al.* A single-molecule diode. *Proc. Natl. Acad. Sci. U. S. A.* **102,** 8815–20 (2005).

75. Díez-Pérez, I. *et al.* Rectification and stability of a single molecular diode with controlled orientation. *Nat. Chem.* **1,** 635–641 (2009).

76. Nijhuis, C. A., Reus, W. F. & Whitesides, G. M. Mechanism of Rectification in Tunneling Junctions Based on Molecules with Asymmetric Potential Drops. *J. Am. Chem. Soc.* **132,** 18386–18401 (2010).

77. Ladilina, E. Y. *et al.* Carbofunctional fluorine-containing triethoxysilanes: synthesis, film forming and properties. *Russ. Chem. Bull.* **54,** 1160–1168 (2005).

78. Hicks, J. C., Dabestani, R., Buchanan, A. C. & Jones, C. W. Spacing and site isolation of amine groups in 3-aminopropyl-grafted silica materials: The role of protecting groups. *Chem. Mater.* **18,** 5022–5032 (2006).

79. Porter, M. D., Bright, T. B., Allara, D. L. & Chidsey, C. E. D. Spontaneously organized molecular assemblies. 4. Structural characterization of n-alkyl thiol monolayers on gold by optical ellipsometry, infrared spectroscopy, and electrochemistry. *J. Am. Chem. Soc.* **109,** 3559–3568 (1987).

80. Pernstich, K. P. *et al.* Threshold voltage shift in organic field effect transistors by dipole monolayers on the gate insulator. *J. Appl. Phys.* **96,** 6431–6438 (2004).

81. Coll, M. *et al.* Formation of Silicon-Based Molecular Electronic Structures Using Flip-Chip Lamination. *J. Am. Chem. Soc.* **131,** 12451–12457 (2009).

82. Ward, J. W. *et al.* Tailored interfaces for self-patterning organic thin-film transistors.

J. Mater. Chem. **22,** 19047 (2012).

83. Kresse, G. & Joubert, D. From ultrasoft pseudopotentials to the projector augmented-wave method. *Phys. Rev. B* **59,** 1758–1775 (1999).

84. Nijhuis, C. A., Reus, W. F., Barber, J. R., Dickey, M. D. & Whitesides, G. M. Charge Transport and Rectification in Arrays of SAM-Based Tunneling Junctions. *Nano Lett.* **10,** 3611–3619 (2010).

85. Wimbush, K. S. *et al.* Control over Rectification in Supramolecular Tunneling Junctions. *Angew. Chemie Int. Ed.* **49,** 10176–10180 (2010).

86. Nijhuis, C. A., Reus, W. F., Siegel, A. C. & Whitesides, G. M. A Molecular Half-Wave Rectifier. *J. Am. Chem. Soc.* **133,** 15397–15411 (2011).

87. Reus, W. F., Thuo, M. M., Shapiro, N. D., Nijhuis, C. A. & Whitesides, G. M. The SAM, Not the Electrodes, Dominates Charge Transport in Metal-Monolayer//Ga_2O_3/Gallium–Indium Eutectic Junctions. *ACS Nano* **6,** 4806–4822 (2012).

88. Lefèvre, X. *et al.* Influence of Molecular Organization on the Electrical Characteristics of π-Conjugated Self-Assembled Monolayers. *J. Phys. Chem. C* **119,** 5703–5713 (2015).

89. Jiang, L., Sangeeth, C. S. S., Wan, A., Vilan, A. & Nijhuis, C. A. Defect Scaling with Contact Area in EGaIn-Based Junctions: Impact on Quality, Joule Heating, and Apparent Injection Current. *J. Phys. Chem. C* **119,** 960–969 (2015).

90. Capozzi, B. *et al.* Single-molecule diodes with high rectification ratios through environmental control. *Nat. Nanotechnol.* **10,** 522–527 (2015).

91. Garg, K. *et al.* Silicon-pyrene/perylene hybrids as molecular rectifiers. *Phys. Chem. Chem. Phys.* **17,** 1891–1899 (2015).

92. Luo, L. *et al.* Hopping Transport and Rectifying Behavior in Long Donor–Acceptor Molecular Wires. *J. Phys. Chem. C* **118,** 26485–26497 (2014).

93. Mativetsky, J. M., Loo, Y.-L. & Samorì, P. Elucidating the nanoscale origins of organic electronic function by conductive atomic force microscopy. *J. Mater. Chem. C* **2,** 3118–3128 (2014).

94. Cui, B. *et al.* Effect of geometrical torsion on the rectification properties of diblock conjugated molecular diodes. *J. Appl. Phys.* **116,** 073701 (2014).

95. Mativetsky, J. M. *et al.* Azobenzenes as Light-Controlled Molecular Electronic Switches in Nanoscale Metal−Molecule−Metal Junctions. *J. Am. Chem. Soc.* **130,** 9192–9193 (2008).

96. Chen, X. *et al.* Molecular diodes with rectification ratios exceeding 105driven by electrostatic interactions. *Nat. Nanotechnol.* **12,** 797–803 (2017).

97. Lamport, Z. A. *et al.* Fluorinated benzalkylsilane molecular rectifiers. *Sci. Rep.* **6,** 38092 (2016).

98. Ng, M. K., Lee, D. C. & Yu, L. Molecular diodes based on conjugated diblock co-oligomers. *J. Am. Chem. Soc.* **124,** 11862–11863 (2002).

99. Yuan, L. *et al.* Controlling the direction of rectification in a molecular diode. *Nat. Commun.* **6,** 6324 (2015).

100. Jin, Y., Friedman, N., Sheves, M. & Cahen, D. Effect of Metal−Molecule Contact

Roughness on Electronic Transport: Bacteriorhodopsin-Based, Metal–Insulator–Metal Planar Junctions. *Langmuir* **24,** 5622–5626 (2008).

101. Kuikka, M. A., Li, W., Kavanagh, K. L. & Yu, H.-Z. Nanoscale Electrical and Structural Characterization of Gold/Alkyl Monolayer/Silicon Diode Junctions. *J. Phys. Chem. C* **112,** 9081–9088 (2008).

102. Zhao, J., Yu, C., Wang, N. & Liu, H. Molecular Rectification Based on Asymmetrical Molecule−Electrode Contact. *J. Phys. Chem. C* **114,** 4135–4141 (2010).

103. Nguyen, Q. van *et al.* Control of Rectification in Molecular Junctions: Contact Effects and Molecular Signature. *J. Am. Chem. Soc.* **139,** 11913–11922 (2017).

104. Song, P., Yuan, L., Roemer, M., Jiang, L. & Nijhuis, C. A. Supramolecular vs Electronic Structure: The Effect of the Tilt Angle of the Active Group in the Performance of a Molecular Diode. *J. Am. Chem. Soc.* **138,** 5769–5772 (2016).

105. Batterjee, S. M., Marzouk, M. I., Aazab, M. E. & El-Hashash, M. A. The electrochemistry of some ferrocene derivatives: redox potential and substituent effects. *Appl. Organomet. Chem.* **17,** 291–297 (2003).

106. Hegner, M., Wagner, P. & Semenza, G. Ultralarge atomically flat template-stripped Au surfaces for scanning probe microscopy. *Surf. Sci.* **291,** 39–46 (1993).

107. Shao, Y. *et al.* Synthesis, characterization and catalytic activity of acid–base bifunctional materials by controlling steric hindrance. *Microporous Mesoporous Mater.* **128,** 120–125 (2010).

108. Halik, M. *et al.* Low-voltage organic transistors with an amorphous molecular gate dielectric. *Nature* **431,** 963–966 (2004).

109. Collet, J., Tharaud, O., Chapoton, A. & Vuillaume, D. Low-voltage, 30 nm channel length, organic transistors with a self-assembled monolayer as gate insulating films. *Appl. Phys. Lett.* **76,** 1941 (2000).

110. Klauk, H., Zschieschang, U., Pflaum, J. & Halik, M. Ultralow-power organic complementary circuits. *Nature* **445,** 745–748 (2007).

111. DiBenedetto, S. A., Facchetti, A., Ratner, M. A. & Marks, T. J. Molecular Self-Assembled Monolayers and Multilayers for Organic and Unconventional Inorganic Thin-Film Transistor Applications. *Adv. Mater.* **21,** 1407–1433 (2009).

112. Jiang, X. *et al.* Palladium-Catalyzed Formylation of Aryl Halides with *tert* -Butyl Isocyanide. *Org. Lett.* **16,** 3492–3495 (2014).

113. Dauselt, J. *et al.* Compensation of the Odd−Even Effects in Araliphatic Self-Assembled Monolayers by Nonsymmetric Attachment of the Aromatic Part. *J. Phys. Chem. C* **115,** 2841–2854 (2011).

114. Saito, M. *et al.* One-step synthesis of [1]benzothieno[3,2-b][1]benzothiophene from o-chlorobenzaldehyde. *Tetrahedron Lett.* **52,** 285–288 (2011).

115. Košata, B., Kozmík, V. & Svoboda, J. Reactivity of [1]Benzothieno[3,2-b][1]benzothiophene - Electrophilic and Metallation Reactions. *Collect. Czechoslov. Chem. Commun.* **67,** 645–664 (2002).

Curriculum Vitae

ANGELA D. BROADNAX
broaad13@wfu.edu
www.linkedin.com/in/angelabroadnax

EDUCATION

Wake Forest University, Winston Salem, NC
Ph.D., Chemistry-Organic Division, August 2018

University of North Carolina at Chapel Hill, Chapel Hill, NC
M.S., Chemistry-Biological Division, August 2013

North Carolina Agricultural & Technical State University, Greensboro, NC
M.S., Chemistry, May 2009
B.S., Chemistry ACS, May 2006

TEACHING EXPERIENCE

Wake Forest University
Organic Chemistry Lab Graduate Teaching Assistant December 2013-Present
Teaching concepts, supervising and assisting undergraduate students in lab, lab reports, and holding office hours to provide students with additional class support. Also, taught prelab on radical polymerization (April, 2017).

Wake Forest University
Chemistry Center Instructor August 2017-November 2017
Assisted students in learning chemical concepts, problem-solving strategies, and answered general questions.

Wake Forest University
Organic Chemistry Guest Lecturer February and April 2016
Taught the following topics: alkenes, stereoisomerism, and Mass Spec/NMR.

Wake Forest University
Organic Chemistry Guest Lecturer August 4-5, 2015
Taught the following topics: NMR spectroscopy and synthesis.

UNC-Chapel Hill
Organic Chemistry Lab Graduate Teaching Assistant August 2012-July 2013
Taught and supervised undergraduate students, graded exams and lab reports, proctored exams, and held weekly office hours to provide students with additional class support.

RESEARCH AND PROFESSIONAL EXPERIENCE

Advisor: Dr. Mark Welker, Wake Forest University — Winston Salem, NC
Chemistry Department, Organic Division — expected May 2018
5th year Graduate Student
Research Description: Synthesis of benzyalkylsilanes as molecular rectifiers

Advisor: Dr. Mark Schoenfisch, UNC-Chapel Hill — Chapel Hill, NC
Chemistry Department, Biological Division — August 2010-May 2013
Graduate Student
Research Description: Synthesis and characterization of nitric oxide-releasing silica particles (Published article on this work shown below)

Scynexis — Research Triangle Park, NC
Scynexis Medicinal Chemistry Intern — May 2010-August 2010
Collaborated with the Drugs for Neglected Disease initiative in an effort to discover and develop affordable and effective therapies for Human African Trypanosomiasis.

Advisor: Dr. Matthew Redinbo, UNC-Chapel Hill
Chemistry Department — Chapel Hill, NC
Research Assistant — September 2009-May 2010
Cloning, protein purification and biochemical characterization of *Kingella kingae* proteins pilC1 and pilC2 (Published article on this work shown below)

Merck & Co. — West Point, PA
Merck Future Talent/ADC Specialty Intern — June 2009-August 2009
Authored an extensive 130 page user's manual for the Automated Statistical Analysis and Reporting Tool for Stability Data (ASARTS). Interviewed ASARTS users, presented an ASARTS PowerPoint presentation to the ADC Specialty group

Advisor: Dr. Marion Franks, NC A&T State University
Chemistry Department
Graduate Student — August 2006-May 2009
M.S. Thesis: *The Synthesis of Boronate Ester Coumarins as Chemopreventives*, 2009
Research Description: Prepared three boronate ester coumarins, including two novel compounds, to be used as anticancer agents

PUBLICATIONS

A. D. Broadnax, Z.L. Lamport, O.D. Jurchescu, M.E. Welker, "Ferrocenealkylsilane molecular rectifiers," *Journal of Organometallic Chemistry*., **2018**, 856, 23-26.

Z.L. Lamport, **A. D. Broadnax**, D. Harrison, K.J. Barth, L. Mendenhall, C.T. Hamilton, M. Guthold, T. Thonhauser, M.E. Welker, O.D. Jurchescu, "Fluorinated benzalkysilane molecular rectifiers," *Scientific Reports*., **2016**, 6, 1-7.

A. D. Broadnax, Z.L. Lamport, L. Mendenhall, M.E. Welker, O.D. Jurchescu, "Fluorinated benzalkylsilanes as molecular rectifiers", **2016 SERMACS oral presentation.**

A. D. Broadnax, Z.L. Lamport, L. Mendenhall, M.E. Welker, O.D. Jurchescu, "Triethoxysilyalkyl-fluorinatedphenylmethanimine Self-Assembled Monolayers as Molecular Rectifiers", **2015, 2016, NOBCChE poster presentation**.

D.L. Slomberg, Y. Lu, **A. D. Broadnax**, R.A. Hunter, A.W. Carpenter, and M.H. Schoenfisch, "Role of Size and Shape on Biofilm Eradication for Nitric Oxide-Releasing Silica Nanoparticles," *ACS Appl. Mater. Interf*aces., **2013**, 5, 9322-9329.

E. A. Porsch, M. D. L. Johnson, **A. D. Broadnax**, C. K. Garrett, M. R. Redinbo, and J. W. St. Geme III,
"Calcium Binding Properties of the *Kingella kingae* PilC1and PilC2 Proteins Have Differential Effects on Type IV Pilus-Mediated Adherence and Twitching Motility", *J. Bacteriol*., **2013**, 195:4, 886−895.

B. J. Privett, **A. D. Broadnax**, S. J. Bauman, D. A. Riccio, M. H. Schoenfisch, "Examination of Bacterial Resistance to Exogenous Nitric Oxide", *Nitric Oxide*., **2012**, 26, 169−173.

D. A. Riccio, P. N. Coneski, S. P. Nichols, **A. D. Broadnax**, M. H. Schoenfisch, "Photoinitiated Nitric Oxide-Releasing Tertiary *S*-Nitrosothiol-Modified Xerogels", *ACS Appl. Mater. Interfaces*., **2012**, 4, 796−804.

AWARDS

2017 Outstanding Teaching Assistant of the Year	2017
Graduate Pilot Research Grant (Chemistry Department)	2017
Travel Support (Chemistry Department)	2015 and 2017
WFU Alumni Student Travel Award	2015-2017
NOBCChE Travel Award	2015, 2016
NC Alliance to Create Opportunity through Education Fellowship	2008-2009
Chemistry Student of the Year	2006
Alpha Lambda Delta Honoree	2003
NC A&T Honors Program Participant	2002-2006
Gateway for Advancing Science and Mathematics Scholarship	2002-2006

MEMBERSHIPS

American Chemical Society (ACS)	2015-present
Graduate Student Association (secretary)	2015-2016
National Organization for the Advancement of Black Chemists And Chemical Engineers (NOBCChE)	2015-2017
Iota Sigma Pi National Honor Society for Women in Chemistry	2012-2013